New
Phytologist

Expression quantitative trait loci mapping identified *PtrXB38* as a key hub gene in adventitious root development in *Populus*

Tao Yao[1,2]*, Jin Zhang[1,2,3]*, Timothy B. Yates[1,2,4], Him K. Shrestha[1,5], Nancy L. Engle[1,2], Raphael Ployet[1,2], Cai John[1,2,4], Kai Feng[1,2], William Patrick Bewg[2,6,7,8], Margot S. S. Chen[6,7,8], Haiwei Lu[1,9], Scott A. Harding[6,7,8], Zhenzhen Qiao[1], Sara S. Jawdy[1,2], Mengjun Shu[1,2], Wenya Yuan[3], Khadijeh Mozaffari[6,7,8], Anne E. Harman-Ware[2,10], Renee M. Happs[2,10], Larry M. York[1,2], Brad M. Binder[11], Yuko Yoshinaga[12], Christopher Daum[12], Timothy J. Tschaplinski[1,2], Paul E. Abraham[1,2], Chung-Jui Tsai[2,3], Kerrie Barry[12], Anna Lipzen[12], Jeremy Schmutz[12,13], Gerald A. Tuskan[1,2], Jin-Gui Chen[1,2] and Wellington Muchero[1,2]

[1]Biosciences Division, Oak Ridge National Laboratory, Oak Ridge, TN 37831, USA; [2]Center for Bioenergy Innovation, Oak Ridge National Laboratory, Oak Ridge, TN 37831, USA; [3]State Key Laboratory of Subtropical Silviculture, College of Forestry and Biotechnology, Zhejiang A&F University, Hangzhou, 311300, China; [4]Bredesen Center for Interdisciplinary Research, University of Tennessee, Knoxville, TN 37996, USA; [5]Graduate School of Genome Science and Technology, University of Tennessee, Knoxville, TN 37996, USA; [6]Warnell School of Forestry and Natural Resources, University of Georgia, Athens, GA 30602, USA; [7]Department of Genetics, University of Georgia, Athens, GA 30602, USA; [8]Department of Plant Biology, University of Georgia, Athens, GA 30602, USA; [9]Department of Academic Education, Central Community College – Hastings, Hastings, NE 68902, USA; [10]Renewable Resources and Enabling Sciences Center, National Renewable Energy Laboratory, Golden, CO 80401, USA; [11]Department of Biochemistry & Cellular and Molecular Biology, University of Tennessee, Knoxville, TN 37996, USA; [12]US Department of Energy Joint Genome Institute, Lawrence Berkeley National Laboratory, Berkeley, CA 94720, USA; [13]HudsonAlpha Institute for Biotechnology, Huntsville, AL 35806, USA

Authors for correspondence:
Jin-Gui Chen
Email: chenj@ornl.gov

Wellington Muchero
Email: mucherow@ornl.gov

Summary

- Plant establishment requires the formation and development of an extensive root system with architecture modulated by complex genetic networks.
- Here, we report the identification of the *PtrXB38* gene as an expression quantitative trait loci (eQTL) hotspot, mapped using 390 leaf and 444 xylem *Populus trichocarpa* transcriptomes. Among predicted targets of this *trans*-eQTL were genes involved in plant hormone responses and root development.
- Overexpression of *PtrXB38* in *Populus* led to significant increases in callusing and formation of both stem-born roots and base-born adventitious roots. Omics studies revealed that genes and proteins controlling auxin transport and signaling were involved in PtrXB38-mediated adventitious root formation. Protein–protein interaction assays indicated that PtrXB38 interacts with components of endosomal sorting complexes required for transport machinery, implying that PtrXB38-regulated root development may be mediated by regulating endocytosis pathway.
- Taken together, this work identified a crucial root development regulator and sheds light on the discovery of other plant developmental regulators through combining eQTL mapping and omics approaches.

Introduction

The expression quantitative trait loci (eQTL) analysis approach is a powerful tool used to link genetic variation across accessions with different genomic polymorphisms with gene expression levels. This approach has been widely used to uncover the genetic architecture of transcriptional regulation and to predict phenotypic variation (Cubillos *et al.*, 2012; Wade *et al.*, 2022). In poplar, eQTL mapping has been particularly useful for identifying the genomic hotspots involved in defense response and lignin biosynthesis (Zhang *et al.*, 2018; Balmant *et al.*, 2020). Moreover,

tissue-specific eQTL analyses can be used to unravel the transcriptional regulatory networks during organ differentiation. By analyzing eQTLs in specific tissues, researchers can identify the regulatory mechanisms that govern gene expression in different organs. This approach can also reveal pleiotropic hotspots that function in multiple organs, providing a deeper understanding of the genetic basis of complex traits (Drost *et al.*, 2010). Combining the eQTL approach with other omics approaches can further enhance our understanding of the regulatory mechanisms underlying complex traits (Xiao *et al.*, 2021; Zhang *et al.*, 2023).

Adventitious roots are derived from post-embryonic cells and formed in non-root organs, such as stems and leaves. They can be part of developmental programs or induced by adverse

*These authors contributed equally to this work.

environmental conditions (Bellini *et al.*, 2014; Steffens & Rasmussen, 2015). Adventitious roots produced from the stem, such as crown roots, are referred to as stem-born roots (Bellini *et al.*, 2014). Recently, SHOOTBORNE ROOTLESS (SBRL) was identified as a specific regulator of stem-born root formation in tomato. *SRBL* encodes a clade IIIB LATERAL ORGAN BOUNDARIES DOMAIN (LBD) type transcription factor. In combination with IIIA LBD genes, they form an evolutionarily conserved superlocus controlling both adventitious and lateral root formation (Omary *et al.*, 2022).

In addition to stem-born roots, adventitious roots can also be developed at stem base of *in vitro* cuttings, and we refer this type of adventitious roots as base-born roots. Molecular mechanisms underlying base-born root initiation and growth have been studied over the last decades, and several genes have been cloned as positive or negative regulators. For instance, several transcription factors, including WUSCHEL-related homeobox (WOX) and SCARECROW/SHORT-ROOT (SCR/SHR) family members, were characterized to act in promoting adventitious root formation in *Populus* (Xuan *et al.*, 2014; Xu *et al.*, 2015). Small RNAs and short peptides were also recently identified as playing important roles in adventitious root formation and growth in *Populus* (Cai *et al.*, 2019; Yue *et al.*, 2020; Xu *et al.*, 2021).

Adventitious root formation and growth are regulated by environmental conditions, such as light and nutrients, as well as endogenous plant signals, such as plant hormones (Bellini *et al.*, 2014). Auxin is a central regulator that controls the initiation and growth of adventitious roots. Auxin biosynthesis genes, such as *YUCCA FLAVIN MONOOXYGENASE-LIKE 1* (*YUC1*), *YUC2*, *YUC4*, and *YUC6*, were shown to play important roles in adventitious root generation in *Arabidopsis* (Lakehal & Bellini, 2019). Polar auxin transport, mediated by AUXIN1/LIKE-AUX (AUX/LAX), PIN-FORMED (PIN), and ATP-binding cassette family B (ABCB) proteins, is crucial for plant growth and development including adventitious root formation in rice (Steffens & Rasmussen, 2015). AUX/LAX proteins are auxin influx carriers while PIN proteins are auxin efflux carriers, and some ABCB proteins, such as ABCB1, ABCB4, and ABCB19, mediate both auxin influx and efflux (Petrášek & Friml, 2009; Geisler *et al.*, 2017). It is worth mentioning that PINs and ABCBs are regulated by the endocytosis pathway, in which PINs experience constitutive recycling and degradation between the plasma membrane and the TRANS Golgi network/early endosome (TGN/EE) (Kleine-Vehn & Friml, 2008). The post-translational modification and degradation of PIN proteins are regulated by the subunits of the endosomal sorting complexes required for transport (ESCRT) complex, such as TOM1-like 3 (TOL3) and FYVE domain protein required for endosomal sorting 1 (FREE1) (Gao *et al.*, 2014, 2017; Moulinier-Anzola *et al.*, 2020). In addition to auxin, ethylene was reported to enhance adventitious root formation but reduce root length in petunia, tomato, and *Populus* cuttings, suggesting that extensive hormone cross-talks play roles during adventitious root formation (Druege *et al.*, 2016; Bannoud & Bellini, 2021).

XB3 was first identified as an Xa21-interacting ubiquitin ligase, which consists of both ankyrin (ANK) repeats and a RING finger domain that contribute to Xa21 protein stability and *Xanthomonas oryzae* pv *oryzae* disease resistance in rice (Wang *et al.*, 2006). The XB3 ortholog in *Arabidopsis thaliana* (XBAT) family contains five members in *Arabidopsis*, XBAT31 to XBAT35 (Nodzon *et al.*, 2004). XBAT32 has been reported to regulate lateral root development by targeting ethylene biosynthesis and auxin transport (Nodzon *et al.*, 2004; Prasad *et al.*, 2010). XBAT31 and XBAT35 were found to be involved in thermomorphogenesis by degrading ELF3 proteins (Zhang *et al.*, 2021a,b). *XBAT35* has two splicing variants, *XBAT35.1* and *XBAT35.2*, which encode proteins with different subcellular localizations, nucleus, and cytoplasm, respectively (Carvalho *et al.*, 2012). XBAT35.2 was further validated to be predominantly localized in Golgi apparatus (Liu *et al.*, 2017). Non-nuclear-localized XBAT35.2 was shown to regulate ethylene-mediated apical hook curvature as well as responses to biotic and abiotic stresses (Carvalho *et al.*, 2012; Liu *et al.*, 2017; Li *et al.*, 2020; Yu *et al.*, 2020).

Clonal propagation is a commonly utilized technique in horticulture, agriculture, and forestry because it is an economically efficient method. The formation and growth of adventitious roots are essential for the success of clonal propagation for perennial tree species (Díaz-Sala, 2020). *Populus* is a model perennial woody species with extensive genomic and genetic resources (Tuskan *et al.*, 2006; Muchero *et al.*, 2018). Taking advantage of *Populus* natural variation and transcriptomics data, we aim to identify genetic determinants of plant growth and development and elucidate the underlying transcriptional regulatory networks using eQTL methods. In this study, we identified XB3 family protein 8 in *Populus trichocarpa* (PtrXB38), as a key hub gene of root development and plant hormone signaling in *Populus*. We demonstrated that PtrXB38 regulates both stem-born and base-born adventitious root formation. Omics studies revealed that endogenous plant hormones especially auxin signaling play crucial roles in PtrXB38-mediated adventitious root formation.

Materials and Methods

eQTL mapping

Whole-genome resequencing and variant calling for the 917 *P. trichocarpa* Torr. & Gray individuals was performed as described previously (Yates *et al.*, 2021). The single nucleotide polymorphism (SNP) and indel dataset is available at http://bioenergycenter.org/besc/gwas/. A total of 390 and 444 RNA-Seq samples in leaf and xylem, respectively, were used to perform eQTL analysis. Prepublication RNA-seq data were made available for this study courtesy of the Center for Bioenergy Innovation and the Joint Genome Institute. Briefly, leaf and xylem tissue were collected in 2015 from 4-yr-old trees at the Clatskanie, OR field site and processed as described previously (Zhang *et al.*, 2018). Reads were aligned to the *P. trichocarpa* v.3.1 reference genome (Tuskan *et al.*, 2006), using STAR (Dobin *et al.*, 2013). Fragments per kilobase of transcript per million mapped reads (FPKM) counts were then obtained for each genotype, resulting in a genotype–transcript matrix. The association

between gene expression profiles and SNPs was tested using EMMAX (Zhou & Stephens, 2012). SNPs and InDels with minor allele frequencies ≥ 0.05 identified from whole-genome resequencing were used for this analysis. To account for multiple testing, we used the Bonferroni corrected threshold, $P \leq 0.05/8253\,066 = 6.06 \times 10^{-9}$, to determine statistical significance. For the hub eQTL, the significant eQTLs that associated with > 500 genes expression were identified as hub eQTLs. The eQTL network was then created around the *PtrXB38* using CIRCOS (Krzywinski *et al.*, 2009).

Phylogenetic analysis of PtrXB38

The full-length XB3 amino acid sequences from four species (*P. trichocarpa*, *A. thaliana* (L.) Heynh, *Oryza sativa* L., and *Physcomitrella patens* (Hedw.) B., S. & G.) were aligned with the MUSCLE algorithm in MEGA X (Kumar *et al.*, 2018). The interspecific phylogenetic trees were subsequently constructed in MEGA X using the maximum likelihood (ML) method with 100 bootstrap replications or neighbor joining (NJ) method with 1000 bootstrap replications.

Bioinformatics analysis for PtrXB3 family

Domain predictions of PtrXB3 proteins were performed using PFAM and SMART tools (Letunic *et al.*, 2020; Mistry *et al.*, 2020), and the results were visualized by EVOLVIEW (Subramanian *et al.*, 2019). Normalized expression values of the PtrXB3 genes from various tissues and organs were obtained from the *Populus* Gene Atlas database (https://phytozome-next.jgi.doe.gov/phytomine/aspect.do?name=Expression). Heatmapper was used to visualize the expression pattern (Babicki *et al.*, 2016).

Generation of *PtrXB38-OE* and -*KO* plants in *Populus*

The full-length coding sequence of *PtrXB38* (Potri.010G070800.6) was PCR amplified from xylem cDNA of *P. trichocarpa* 'Nisqually-1' (see Supporting Information Table S1 for primers) and assembled into the binary vector p201N-Cas9 (plasmid 59175; Addgene, Cambridge, MA, USA) (Jacobs *et al.*, 2015) to replace *SpCas9* behind the double 35S promoter using the NEBuider HiFi DNA assembly cloning kit (New England Biolabs, Ipswich, MA, USA). The generation and genotyping of *PtrXB38-KO* transgenic *Populus* plants in *P. tremula* L. × *alba* L. IRNA 717-1B4 followed the methods as described (Bewg *et al.*, 2022). Briefly, to generate the *PtrXB38* knockout (KO) construct, SwaI-digested p201N-Cas9 vector was PCR amplified by Q5 High-Fidelity DNA Polymerase (New England BioLabs) with primers listed in Table S1. The *MtU6.6* promoter and scaffold fragments were also PCR amplified from the pUC-gRNA shuttle vector (plasmid 47024; Addgene) (Jacobs *et al.*, 2015) using tailed primers overlapping with p201N (Table S1). The p201N-Cas9 vector, *U6.6* promoter, scaffold, and a pair of tailed primers containing the gRNA sequence were then assembled together using NEBuilder HiFi DNA Assembly Cloning Kit (New England Biolabs). Both constructs were fully sequenced and heat-shock transformed into *Agrobacterium tumefaciens* strain

C58/GV3101 (pMP90) (Koncz & Schell, 1986). The *Populus* transformation and regeneration was performed as described (Bewg *et al.*, 2022).

Mutation patterns were determined by amplicon sequencing as described (Bewg *et al.*, 2022). Gene-specific degenerate primers (Table S1) flanking both on-target (Potri.010G070800) and off-target (genome duplicate Potri.008G167600) sites were used for the first PCR, followed by PCR-barcoding, both using GoTaq G2 Green Master Mix (Promega). The pooled amplicon library was quantified by a Qubit Fluorometer (Invitrogen) before being sequenced on an Illumina MiSeq (Illumina, San Diego, CA, USA) using a Nano PE150 flow cell at the Georgia Genomics and Bioinformatics Core, University of Georgia. After de-multiplexing, data were analyzed by the AGESEQ program (Xue & Tsai, 2015).

Plant growth conditions

The tissue culture plants were maintained in ½ Murashige & Skoog media (½MS basal salts, $20\,g\,l^{-1}$ sucrose, $1\times$ Gamborg's B5 vitamin mixture, 0.3% Gelzan) supplemented with $0.1\,mg\,l^{-1}$ IBA and grown in growth chambers (16 h : 8 h, light : dark) with white, fluorescent light ($100\,\mu mol\,m^{-2}\,s^{-1}$) at 22°C. To assess the adventitious root development phenotype, 2–3 cm length of shoot tops from 1-month-old tissue culture saplings were excised and placed in fresh medium for root induction. Root number was counted 12 d after subculturing. For chemical treatment, filter-sterilized auxin transport inhibitor naphthylphthalamic acid (NPA) and ethylene biosynthesis inhibitor aminoethoxyvinylglycine (AVG) were added in the ½MS medium.

Plant imaging and histochemistry

Tissue culture grown *Populus* saplings were imaged using a camera (Nikon D7500; Nikon Corporation, Tokyo, Japan) or stereomicroscope (Zeiss Discovery V8; Zeiss, Jena, Germany). A few millimeters long stem segments were collected and fixed in 80% ethanol. After dehydration in 100% ethanol overnight, samples were embedded in LR White resin (London Resin Co. Ltd, Reading, UK) using consecutive baths of increasing concentrations of resin (1/3, 1/2, 2/3, and 100%). Polymerization was performed at 65°C overnight. Semi-thin sections (1.5 µm-thick) were obtained using a microtome Leica RM2255 (Leica Microsystems, Wetzlar, Germany) equipped with a glass knife, then stained with a solution of Toluidine Blue O (1%, aqueous) and mounted on glass slide using a permanent mounting medium (Cytoseal 60; Thermo Fisher Scientific, Waltham, MA, USA). Images of the sections were captured using an Imager.A2 (Zeiss Discovery V8; Zeiss).

RNA extraction and quantitative RT-PCR analysis

Total RNA was isolated from 7-d-old rooting stem base samples using a Sigma plant total RNA kit according to the manufacturer's instructions. Reverse transcriptional reactions were performed using a SuperScript III kit (Invitrogen) according to the manufacturer's instructions. Quantitative PCR was performed using a StepOne real-time PCR system (Thermo Fisher Scientific) and Maxima

SYBR Green/ROX qPCR master mix (Thermo Fisher Scientific). *PtEF1β* (Potri.009G01860) was used as a reference gene in quantitative RT-PCR and the gene expression level was calculated by the $2^{-\Delta\Delta C_T}$ method (Livak & Schmittgen, 2001). Primers used for quantitative RT-PCR are listed in Table S1.

Transcriptome analysis

Total RNA was isolated from the 12-d-old rooting stem bases, and 1-month-old stem and leaf samples from tissue culture plants using the Sigma plant total RNA kit according to the manufacturer's instructions. Each sample includes three biological replicates. Library construction and sequencing were performed using the DNBseq platform at BGI Genomics Co. Ltd (Shenzhen, China). Clean reads were mapped to the *P. tremula × alba* clone INRA 717-1B4_v.1.1 reference genome with STAR v.2.6.1b (Dobin *et al.*, 2013). FEATURE-COUNTS 1.6.3 in unstranded mode was used to generate raw gene counts, excluding multimapping reads (Zhou & Stephens, 2012). The primary isoform of *PtrXB38* (Potri.010G070800.6) in *P. trichocarpa* was manually curated to correct exon–intron prediction in the 717-1B4 v.1.1 annotation. FPKM normalized counts were generated with RSEM, default parameters were used. DESEQ2 v.1.22.2 was used to identify differentially expressed genes (DEGs; Love *et al.*, 2014). TOPGO was used to generate gene ontology (GO) enrichments and KOBAS was used to generate KEGG enrichments (Alexa *et al.*, 2006; Xie *et al.*, 2011). Heatmaps were generated with TBTOOLS (Chen *et al.*, 2020). For co-expression analysis, a matrix of DEGs in the RNA-seq were constructed by calculating pairwise Pearson correlation coefficients (PCC, *r*). Only significant co-expression relationships with $|r| > 0.80$ and $P \le 0.05$ were indicated in the PCC network.

Proteomics analysis

Proteomics measurements on plant tissues were conducted with three biological replicates, as previously described (Lenz *et al.*, 2022). Briefly, samples were frozen, ground, and solubilized in a lysis buffer. Samples were then boiled, centrifuged, and alkylated. Proteins were extracted using a chloroform–methanol protocol (Jiang *et al.*, 2004) and reconstituted in a sodium deoxycholate (SDC) solution. Proteins were digested with trypsin, and SDC was removed. Peptides were desalted and 20 µg of desalted peptides were aliquoted for LC–MS/MS analysis.

All samples were analyzed using two-dimensional liquid chromatography on an Ultimate 3000 RSLCnano system coupled with a QExactive Plus mass spectrometer (Thermo Scientific, Fremont, CA, USA), as previously described (Wang *et al.*, 2021). MS data were acquired using Thermo XCALIBUR with the topN method. Acquired MS/MS spectra were searched in PROTEOME DISCOVERER v.2.5 using SEQUEST HT (Eng *et al.*, 1994) and PERCOLATOR (Käll *et al.*, 2007). The spectral data were searched against *P. tremula × alba* INRA 717-1B4_v.1.1 database. FDR-controlled peptides were quantified based on chromatographic area under the curve and mapped to proteins. For proteome analysis, the protein table was exported, and proteins were filtered for high confidence and at least two peptide evidence. Quantitative analysis included

transformation, normalization, and mean-centering using INFER-NORDN software (http://omics.pnl.gov/software/infernordn). The data matrix was filtered to remove stochastic sampling. Missing data were imputed using PERSEUS software (Tyanova *et al.*, 2016). Significantly changing proteins were identified through ANOVA and Tukey's HSD test. Further details on proteomics analysis are provided in Supporting Information.

IAA quantification

Root samples were collected were collected from 1-month-old tissue culture plants, snap-frozen in liquid nitrogen, and ground to a fine powder using GenoGrider 2000 sample homogenizer (SPEX Sample Prep, Metuchen, NJ, USA). The frozen powders were shipped to the University of Georgia on dry ice and lyophilized in a FreeZone 4.5 l benchtop freeze dryer (Labconco, Kansas City, MO, USA). Tissue extraction was performed according to Pan *et al.* (2010). Briefly, 5 mg dry weight samples was extracted in 500 µl of extraction solvent (2-propanol : H₂O : HCl, 2 : 1 : 0.002, v/v/v) containing 50 ng d5-IAA (indole-2,4,5,6,7-d5-3-acetic acid; CDN isotopes, Pointe-Claire, QC, Canada) as internal standard. Following incubation with shaking for 30 min at 4°C, 1 ml dichloromethane was added and the samples were incubated with shaking for another 30 min at 4°C before centrifugation. The lower phase was transferred to a new microtube, filtered through 0.22 µm PTFE filters (Agilent Technologies, Wilmington, DE, USA), evaporated under nitrogen, and resuspended in 100 µl MeOH.

The extracts were analyzed on an Agilent 1290 Infinity II ultra-performance liquid chromatography (UPLC) coupled to an Agilent 6546 quadrupole time-of-flight (QTOF) tandem mass spectrometer, using a C18 column (Poroshell 120 EC-C18, 2.1 × 50 mm, 1.9 µm; Agilent Technologies). Mobile phase A consisted of water with 0.05% acetic acid and acetonitrile with 0.05% acetic acid as mobile phase B. Separations were performed in 3 min by changing the percentage of A solvent (Müller & Munné-Bosch, 2011). Flow rate was set to 0.5 ml min⁻¹ and oven temperature to 40°C. Negative polarity data were acquired using MS acquisition mode with the gas temperature 250°C, nebulizer gas 40 psi and capillary voltage 3000 V. The data were analyzed by the Qualitative Analysis Software of Agilent MASSHUNTER WORKSTATION v.10.0. Auxin levels were quantified using a calibration curve built with authentic standard IAA at a range of 20–500 ng ml⁻¹ containing 50 ng d5-IAA as described (Pan *et al.*, 2010). Data were analyzed by the Quantitative Analysis Software v.11.0 of the Agilent MASSHUNTER WORKSTATION.

Subcellular localization assay

The CDS of *PtrXB38* was amplified from *p201N-PtrXB38* vector using Q5 high-fidelity polymerase (New England Biolabs) following the PCR program: 98°C for 30 s, 35 cycles of 98°C for 10 s, 65°C for 30 s, and 72°C for 30 s, with the final elongation step at 72°C for 2 min. The PCR product was cloned into a *pENTR-D/TOPO* vector (Invitrogen) to generate *pENTR-PtrXB38* entry vector. The CDS of *PtrXB38* was cloned into a pGWB505 vector by LR reactions to generate *35S::PtrXB38-GFP* vector. The vector was

co-transfected with Golgi marker (CD3-967) into *P. tremula × alba* protoplasts as described (Nelson *et al.*, 2007; Zhang *et al.*, 2020). GFP and mCherry fluorescences were observed by a Zeiss LSM710 confocal microscope (Zeiss). The excitation/emission wavelengths for GFP and mCherry were 488/505–540 nm and 561/565–610 nm, respectively.

In vitro ubiquitination assay

The CDS of *PtrXB38* from *pENTR-PtrXB38* entry vector was cloned into a *pGEX6P1-DEST* (plasmid 119749; Addgene) vector by LR reactions to generate the *pGEX6P1-PtrXB38* vector. The vector was transformed into *Escherichia coli* Rosetta (DE3) to express GST-PtrXB38 protein. The recombinant protein expression was induced by 0.5 mM isopropyl-b-Dthiogalactoside at 25°C overnight. GST-PtrXB38 protein was purified by MagneGST Glutathione Particles (V8611; Promega) following the manufacturer's instructions. An *in vitro* ubiquitination assay of purified GST-PtrXB38 protein was performed with a kit following the manufacturer's instructions (BML-UW0970-0001; Enzo Life Sciences, Farmingdale, NY, USA). The ubiquitinated proteins were separated on a 7.5% SDS-polyacrylamide gel and immunoblotted with anti-GST (sc-138HRP; Santa Cruz Biotechnology, Santa Cruz, CA, USA) at a 1 : 5000 dilution or anti-Ub antibodies (ADI-SPA-203; Enzo Life Sciences) at a 1 : 1000 dilution. The results were visualized by the use of the ChemiDoc XRS + system (Bio-Rad).

GST-PtrXB38 pull-down and mass spectrometric identification

The pull-down assay was performed with *E. coli* expressed GST-PtrXB38 protein and total proteins extracted from stem or root samples from 1-month-old *P. tremula × alba* wild-type *Populus* plants. Protein extraction and the pull-down assay followed a previous report (Yu *et al.*, 2020). MagneGST Glutathione particles were used to purify PtrXB38 protein complexes. The PtrXB38-interacting protein candidates were identified using the LC–MS/MS service at the Mass Spectrometry Service Center at BGI Americas. Samples were digested and cleaned up using the STrap MS sample prep device according to the manufacturer's protocol (Protifi, Farmingdale, NY, USA). Briefly, samples were reduced, alkylated, and then digested in the STrap device with Lys-C/Trypsin overnight. Digested samples were eluted from the STrap according to the manufacturer's protocol and then dried by a SpeedVac. Each sample was reconstituted with 20 µl mobile phase A. 1 µl of each reconstituted sample was loaded onto the column with a 1-h gradient nano LC–MS/MS system. MS Data were searched against the *P. tremula × alba* INRA 717-1B4_v.1.1 reference proteome database with SEQUEST analysis and AUC workflows to reveal basic protein profiling information.

Bimolecular fluorescence complementation assay

The entry vectors for eight ESCRT subunit genes were generated using a *pENTR-D/TOPO* vector (Invitrogen) with the gBlocks synthesized from IDT (Coraville, IA, USA) or Genescript

(Piscataway, NJ, USA) companies. Bimolecular fluorescence complementation (BiFC) assay was performed in *Populus* protoplasts as described by Shrestha *et al.* (2023). In brief, the CDSs of PtrXB38 and its interacting protein candidates were cloned into CFP^c (pUC119-CD3-1068) and VENUS^n (pUC119-CD3-1076) vectors through Gateway cloning, respectively. A total of 10 µg of CFP^c-PtrXB38 plasmids and 10 µg of VENUS^n-substrate plasmids were co-transfected in *Populus* protoplasts. After 18- to 20-h dark incubation, the reconstructed YFP signals were observed by a Zeiss LSM710 confocal microscope (Zeiss). The excitation/emission wavelengths for YFP and mCherry were 514/517–597 nm.

In vitro pull-down assay

The *MBP-PtrVPS60-010G/PtrTOL3/PtrVPS24-MYC* vectors were generated by LR reactions between the entry vectors of *PtrVPS60-010G/PtrTOL3/PtrVPS24* and *MBP-DC-MYC* destination vector (Park *et al.*, 2018). *In vitro* pull-down assays were performed using *E. coli* expressed GST-PtrXB38 and MBP-PtrVPS60-010G/PtrTOL3/PtrVPS24-MYC proteins following the described method in Cheng *et al.* (2022). Samples were analyzed by SDS-PAGE followed by Western blot analysis using anti-GST at a 1 : 5000 dilution and anti-MYC antibodies (C3956; Sigma-Aldrich) at a 1 : 5000 dilution.

Results

Genetic mapping of the *PtrXB38* gene

In this study, we performed eQTL mapping by association analysis of 390 mature leaf and 444 developing xylem transcriptomes to > 8.2 million SNPs and small InDels in the *P. trichocarpa* population to identify putative upstream regulatory eQTLs. On the basis of association analysis, we identified a *trans*-eQTL hotspot interval (Chr10:9757129–9777959) that was significantly associated with expression of 573 genes in developing xylem and mature leaf transcriptomes (Fig. S1; Table S2). Specifically, 21 SNPs, encompassing a 20.83-kb interval, exhibited associations with expression levels of 492 genes in xylem tissue (*P*-values ≤ 9.85E-11), while 10 SNPs within an overlapping 6.47-kb interval were significantly associated with the expression of 81 genes in leaf tissue (*P*-values ≤ 9.41E-11) (Table S2). After JBrowse scanning, this hotspot eQTL interval is overlapped with the gene body of Potri.010G070800, a C3HC4-type E3 ligase coding gene designated as *PtrXB38* (Yuan *et al.*, 2013). *PtrXB38* belongs to *PtrXB3* gene family which consists of nine members (Fig. S2). All these genes showed similar expression patterns and encode the proteins with ANK domains and a RING domain (Fig. S3). We then analyzed the eQTLs that associated with the expression of *PtrXB38*; noticeably, the expression of *PtrXB38* was strongly regulated by *cis*-eQTL in both leaf and xylem (Fig. 1a–c). In particular, SNP Chr10:9762348 was significantly associated with higher expression of *PtrXB38* in developing xylem and leaf (Fig. 1f,g), as well as expression of its putative targets described later.

Among putative targets for the *PtrXB38 trans*-eQTL were 73 and 18 transcription factors expressed in xylem and leaf,
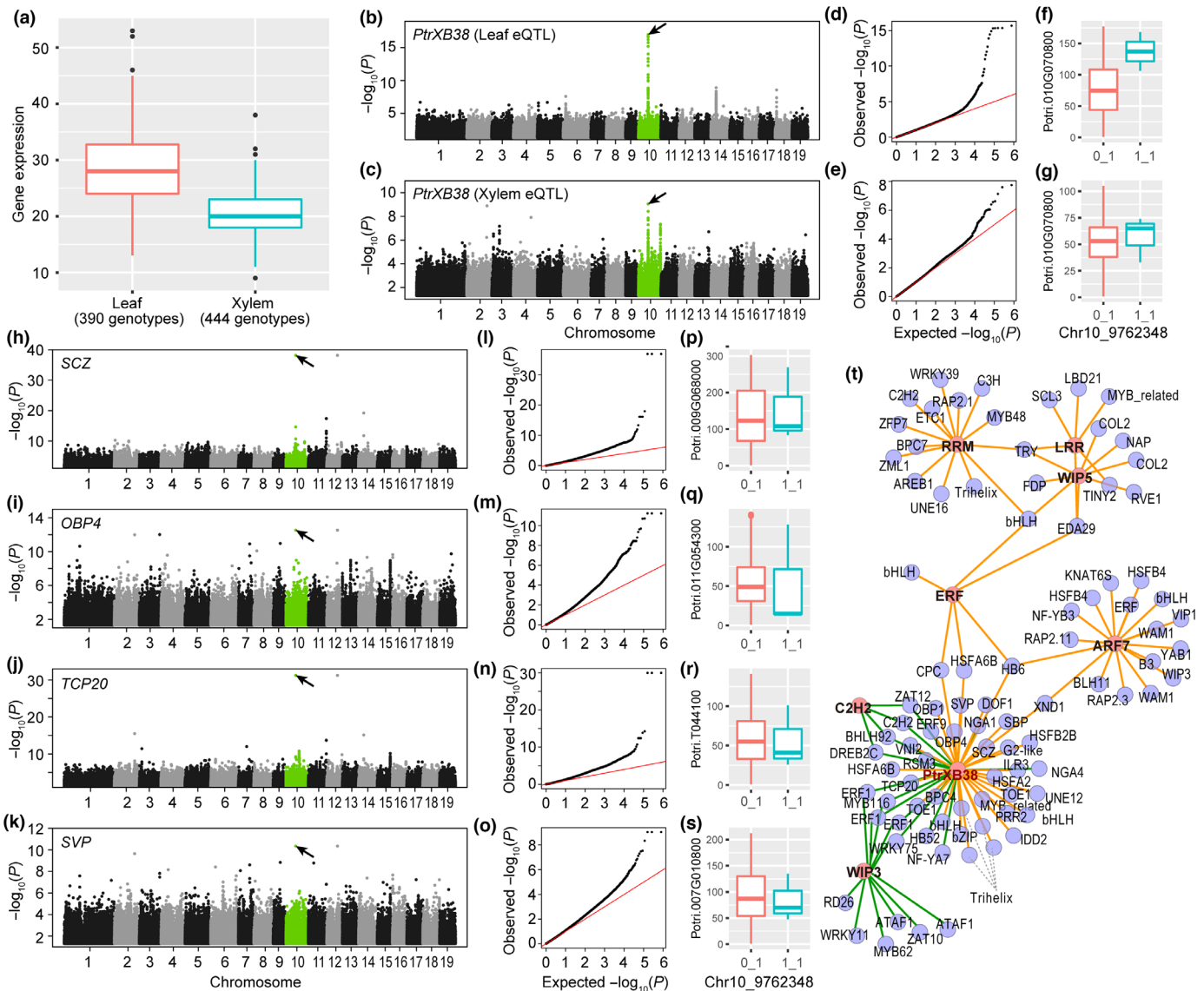
Fig. 1 eQTL mapping identifies PtrXB38 as a developmental regulator in *Populus trichocarpa*. (a) Leaf and xylem expression of *PtrXB38* across *P. trichocarpa* population. (b–e) Manhattan plots and quantile–quantile plots showing the identification of *PtrXB38* as a *cis*-eQTL hotspot in leaf (b, d) and xylem (c, e). Displayed are $-\log_{10}(P \text{ values})$ for association by genomic position. Chromosome (Chr) 10 containing the associated single nucleotide polymorphisms (SNPs) in *PtrXB38* locus is highlighted in green. Chromosomal location of *PtrXB38* is marked with arrows. (f, g) Association of the expression of *PtrXB38* with one of the SNPs at the *PtrXB38* locus, Chr10:9762348, from leaf (f) or xylem (g) transcriptome data. Genotype 0_1 is heterozygous of reference and alternative, and genotype 1_1 is the homozygous alternative. (h–o) Manhattan plots and quantile–quantile plots showing association of the expression of SCZ, OBP4, TCP20, and SVP by genomic position. Chr10 containing the associated SNPs in *PtrXB38* locus is highlighted in green. Chromosomal location of *PtrXB38* is marked with arrows. (p–s) Association of the expression of *SCZ* (p), *OBP4* (q), *TCP20* (r), and *SVP* (s) with one of the SNPs at the *PtrXB38* locus, Chr10:9762348. Genotype 0_1 is heterozygous of reference and alternative, and genotype 1_1 is the homozygous alternative. For the box and whisker plots, the bold line in the center of the boxplots represents the median, the box edges represent the 25th (lower) and 75th (upper) percentiles, and the whiskers extend to the most extreme data points that are no more than 1.5x the length of the upper or lower segment. (t) The TF-based *PtrXB38* regulatory network from eQTL network. The expression profiles of the second layer of TFs were used as phenotypes in the eQTL analysis and the highly associated SNPs flanking genes were extracted as the first layer of regulatory genes. The brown nodes represent the first layer of TFs, and the blue nodes represent the second layer of TFs. The green and orange edges represent the eQTL regulatory relationship was obtained from leaf and xylem dataset, respectively.

respectively (Table S3). These included multiple members of the MYB, APETALA2/ethylene-responsive factor (AP2/ERF), heat shock transcription factor (HSF), basic helix–loop–helix (bHLH), GT and NAM, ATAF1/2, and CUC2 (NAC) families. It is noteworthy that many of these transcription factors were previously identified to regulate plant organ development. Examples include genes previously implicated in callus formation and root

development, such as *SCHIZORIZA* (*SCZ*) and *OBF Binding Protein 4* (*OBP4*) (ten Hove *et al.*, 2010; Ramirez-Parra *et al.*, 2017), as well as regulators of root growth and xylem development, such as *teosinte branched1/cycloidea/proliferating cell factor1-20* (*TCP20*) and *SHORT VEGETATIVE PHASE* (*SVP*) (Li *et al.*, 2005; Zhang *et al.*, 2019) (Fig. 1h–o). Transcript abundance of these genes was significantly associated with SNPs

within the *PtrXB38* locus including Chr10:9762348 mentioned earlier (Fig. 1p–s). Given robust numbers of putatively co-regulated genes in xylem and leaf, we constructed a three-layer network by assessing shared targets among these transcription factors that were associated with *PtrXB38*. Those shared targets may be regulated by *PtrXB38* via these transcription factors. This resulted in a network of putatively co-regulated gene modules falling under the overall regulation of *PtrXB38* (Fig. 1t). Remarkably, auxin response factor (ARF) and ethylene response factor (ERF) transcription factors served as two high-rank nodes in the regulatory network, suggesting that plant hormones, especially auxin and ethylene signaling pathways, are likely involved in *PtrXB38*-regulated developmental processes (Fig. 1t).

PtrXB38 promotes the formation of stem-born roots

Given the number of developmental regulators implicated in the predicted *PtrXB38* regulatory network, we sought to assess its function by generating and characterizing overexpression (OE) and KO transgenic plants in the *P. tremula* × *alba* background (Figs S4, S5). Two independent lines, OE-72 and OE-22, in which the expression of *PtrXB38* was 18- to 90-fold higher, respectively, compared to empty vector control, were selected for further analyses (Fig. S4). In contrast to the control plants, *PtrXB38-OE* plants not only developed larger and more prolific root systems, but also produced more stem-born roots (Fig. 2a,b, d,g). Leaf-born roots were also occasionally observed (Fig. 2a,c,f). Furthermore, a large amount of calli were produced on the stem of *PtrXB38-OE* plants (Figs 2d,e, S5).

To unravel the molecular mechanisms underlying PtrXB38-regulated stem-born roots, we performed transcriptomic analyses on the stem and leaf tissues (Fig. S6). A large number of transcription factor and auxin responsive genes were identified among the DEGs (Tables S4, S5). SBRL was previously identified as a main regulator in stem-born root formation, whose function is conserved among angiosperms (Omary *et al.*, 2022). In line with this finding, we observed that the expression of its orthologs, *LBD17* and *LBD33*, was highly induced in *PtrXB38-OE* plants (Fig. 3a). We also noticed that embryo development-related genes were enriched among the DEGs, indicating that the stem and leaf tissues may experience a dedifferentiation process. We then constructed a co-expression network among *PtrXB38*, *LBD17*, *LBD33*, and other DEGs. The results suggested that LBD17 and LBD33 may have diversified roles as they associated with different sets of DEGs (Fig. 3b). For example, genes associated with *LBD17* expression are hypoxia response related, whereas genes associated with *LBD33* expression are nutrient absorption related (Fig. 3c,d). Nonetheless, the GO enrichment on these two gene sets suggests that basipetal auxin transport plays important roles in stem-born root formation (Fig. 3c,d) (Domagalska & Leyser, 2011). Accordingly, we observed that the expression of genes encoding auxin transporters and response factors was upregulated in *PtrXB38-OE* plants, such as *PIN1*, *ABCB4*, and *ARF5*. These findings were consistent with the quantitative proteomics analysis which showed that protein levels of auxin transporters BIG, PIN1, ABCB1, ABCB4, and

ABCB19, and ARFs, ARF3, ARF4, ARF5, ARF6, ARF7, and ARF8 were also highly accumulated in the stems of *PtrXB38-OE* plants (Fig. 3f; Table S6). Meanwhile, both transcript level and protein abundance of PtrXB38 shown by RNA-seq and proteomics results confirmed that lines OE-72 and OE-22 are *bona fide PtrXB38-OE* plants (Figs S6, S7). Proteomics analysis also revealed that overexpression of *PtrXB38* affected biological processes of vesicular-mediated transport, proteolysis, and small GTPase-mediated signal transduction (Fig. S7c).

PtrXB38 promotes the formation of base-born adventitious roots of microcuttings

In addition to the regulation of stem-born root formation, we wanted to examine whether PtrXB38 regulates the base-born adventitious root formation of microcuttings. During the micropropagation, we excised *c.* 2-cm-long shoot tips and induced adventitious root formation on ½MS medium without IBA. We noticed that the adventitious roots were directly generated from the stem base in control plants while *PtrXB38-OE* plants formed large calli as well as more adventitious roots (Fig. 4a). Quantitatively, *PtrXB38-OE* plants generated 6–12 adventitious roots compared to 3 adventitious roots in control plants (Fig. 4b). The amount of adventitious root formation in the OE lines correlated with the *PtrXB38* transgene expression level (Figs 4a,b, S4). On the other hand, KO mutants of *PtrXB38* did not show any difference in adventitious root formation when compared to control (Fig. S8).

Considering the significant differences in adventitious root formation between OE transgenics and empty vector controls, we assessed transcriptional responses of known wound-induced adventitious root regulators using quantitative RT-PCR analysis on the 7-d-old excised stem bases in ½MS medium. As an early-stage regulator of AR formation, *PtWOX5*, which is expressed in the stem-cell niche and is required for maintaining root meristem activity (Li *et al.*, 2017), was highly upregulated in *PtrXB38-OE* plants (Fig. 4c). In addition, transcript levels of *PtWOX5*'s upstream activator, *PtSHR* (Xuan *et al.*, 2014), were also significantly increased in the *PtrXB38-OE* plants (Fig. 4d). Expression of *AINTEGUMENTA LIKE1 in Populus* (*PtAIL1*), an AP2/ERF family transcription factor gene responsible for root meristem and primordium formation (Rigal *et al.*, 2012), was likewise significantly increased in *PtrXB38-OE* (Fig. 4e). Both *WOX5* and *AIL1* were reported to be involved in auxin-dependent adventitious root development (Druege *et al.*, 2016). In line with this view, we found that *PtrXB38-OE* resulted in upregulation of auxin signaling and transport genes *PtARF15* and *PtPIN1* (Fig. 4f,g). Therefore, results from expression analyses of both stem-born and base-born root formation suggested that auxin signaling and transport are involved in PtrXB38-mediated adventitious root formation.

Involvement of auxin and ethylene signals in PtrXB38-mediated adventitious root formation

To better understand the molecular mechanisms of PtrXB38 in the regulation of adventitious root initiation and development, we performed transcriptome and proteome analyses to identify
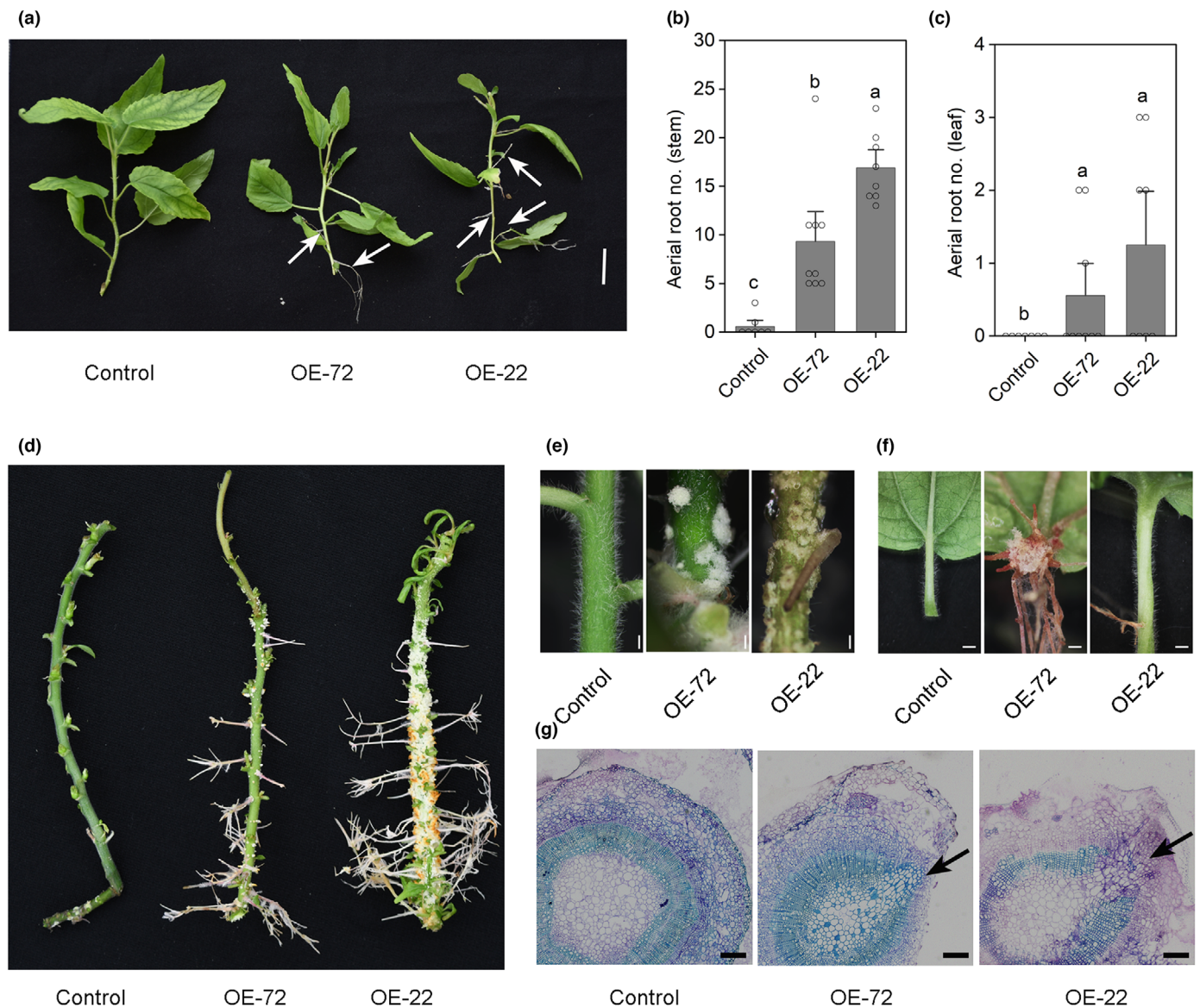
Fig. 2 Overexpression of *PtrXB38* promotes stem-born root formation in poplar (*Populus tremula × Populus alba*). (a) Stem-born root formation on the stem and leaf of 1-month-old control and two *PtrXB38-OE* independent lines, OE-72 and OE-22. The arrows denote the stem-born roots developed from stem or leaf. Bar, 1 cm. (b, c) Adventitious root numbers of 1-month-old control and two *PtrXB38-OE* lines on stem (b) and leaf (c). Bar charts represent mean ± SE ($n \geq 3$ independent plants), and different letters represent significant difference between groups ($P \leq 0.05$) determined by one-way ANOVA followed by Tukey's test. (d) Callus and stem-born root formation on the stem of 3-month-old control and two *PtrXB38-OE* lines. (e, f) Close-up view of calli and roots formed on the stem (e) and leaf (f) of two *PtrXB38-OE* lines. Bars, 1 mm. (g) Stem sectioning of 3-month-old control and *PtrXB38-OE* micropropagated plants. Bars, 200 μm. The arrows denote the initiation sites of stem-born roots.

changes in gene expression and protein abundance specifically in the wound-induced roots of 12-d-old *PtrXB38-OE* plants (Tables S7, S8). Principal component analysis revealed separate clustering of the two *PtrXB38-OE* lines from the control group, reflecting the global transcriptomic and proteomic changes induced by overexpression of *PtrXB38* (Figs S9, S10). Notably, both transcriptome and proteome analyses confirmed the upregulation of many TF families, such as MYB, ERF, and bHLH, supporting the prediction from co-expression analysis described earlier and supporting the identification of *PtrXB38* as a *trans*-eQTL hotspot (Figs 1t, S11). Furthermore, *ARF7* and *ERF.2g*, encoding two key transcription factor genes in auxin and ethylene

signaling pathways, were identified as node genes in the eQTL regulatory network (Fig. 1t). Similarly, they were also identified to be upregulated by *PtrXB38* overexpression from proteomics and RNA-seq analyses (Figs 5a,b, S12a). These findings prompted us to investigate the involvement of plant hormone signaling in PtrXB38-mediated root development.

The DEGs/differentially expressed proteins (DEPs, FDR ≤ 0.05) were further analyzed by GO and Kyoto Encyclopedia of Genes and Genomes (KEGG) pathway enrichments. GO terms 'response to wounding', 'response to auxin', and 'multicellular organism development' were overrepresented (Fig. S13). Similarly, 'regulation of ARF protein signal transduction' was also
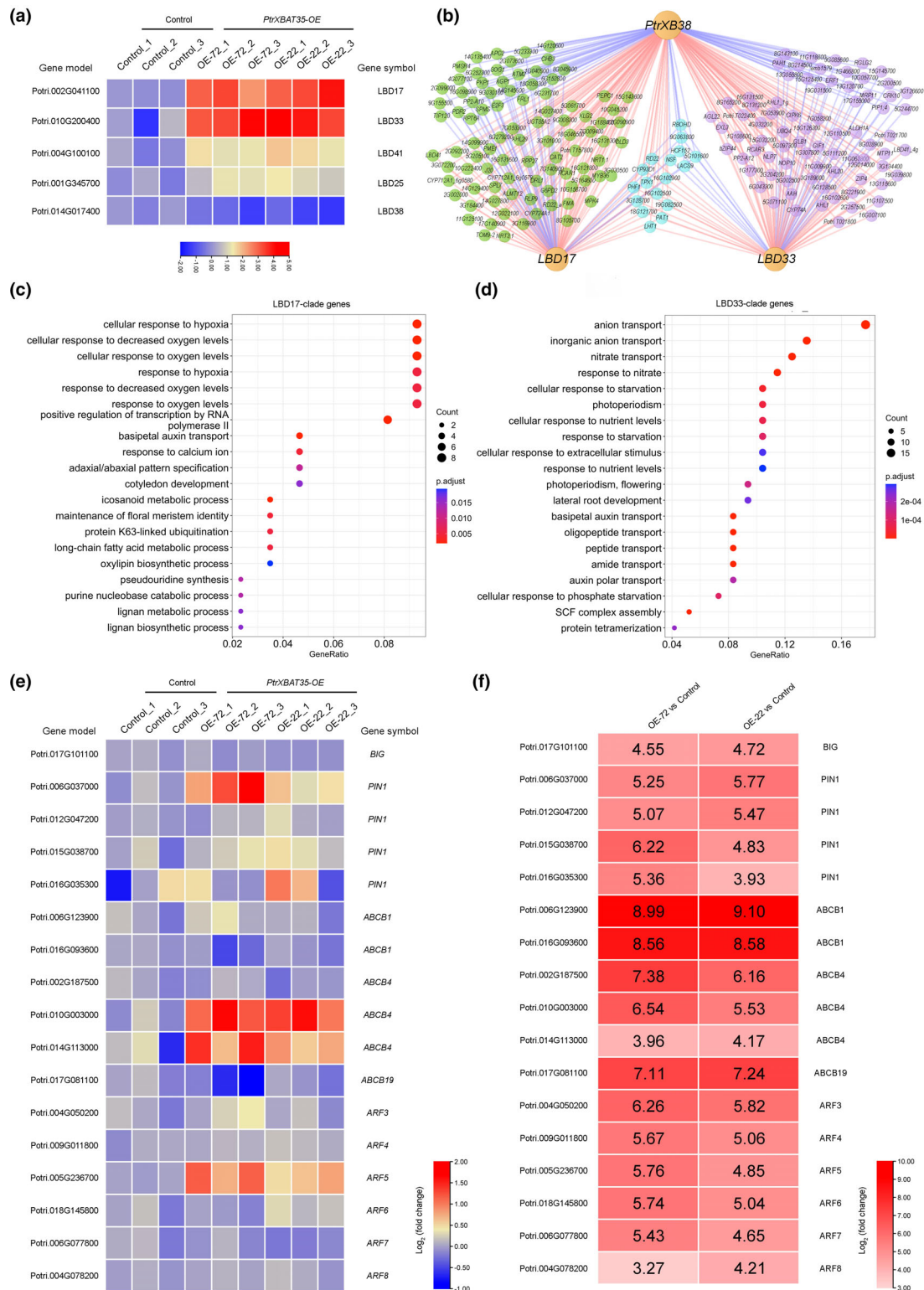
Fig. 3 *LBD* genes associate with *PtrXB38*-mediated stem-born root formation in poplar (*Populus tremula* × *Populus alba*). (a) Relative abundance of transcript of *LBD* genes in the stem of control and two *PtrXB38-OE* independent lines, OE-72 and OE-22. The heatmap is plotted with $\log_2$ (FC) with the FPKM values from RNA-seq results. (b) PCC co-expression analysis of stem RNA-seq dataset. Red and blue lines represent positive and negative correlation, respectively. Green nodes represent genes co-expressed with *LBD17*; purple nodes represent genes co-expressed with *LBD33*. (c) GO annotation of LBD17-clade genes in (b). (d) GO annotation for LBD33-clade genes in (b). (e) Log-fold changes of transcript levels of auxin transport and response-related genes in the stem samples of *PtrXB38-OE* vs control plants, based on RNA-seq dataset. (f) Log-fold changes in protein abundance of auxin transporters and response factors in the stem samples of *PtrXB38-OE* vs control plants, based on quantitative proteomics.
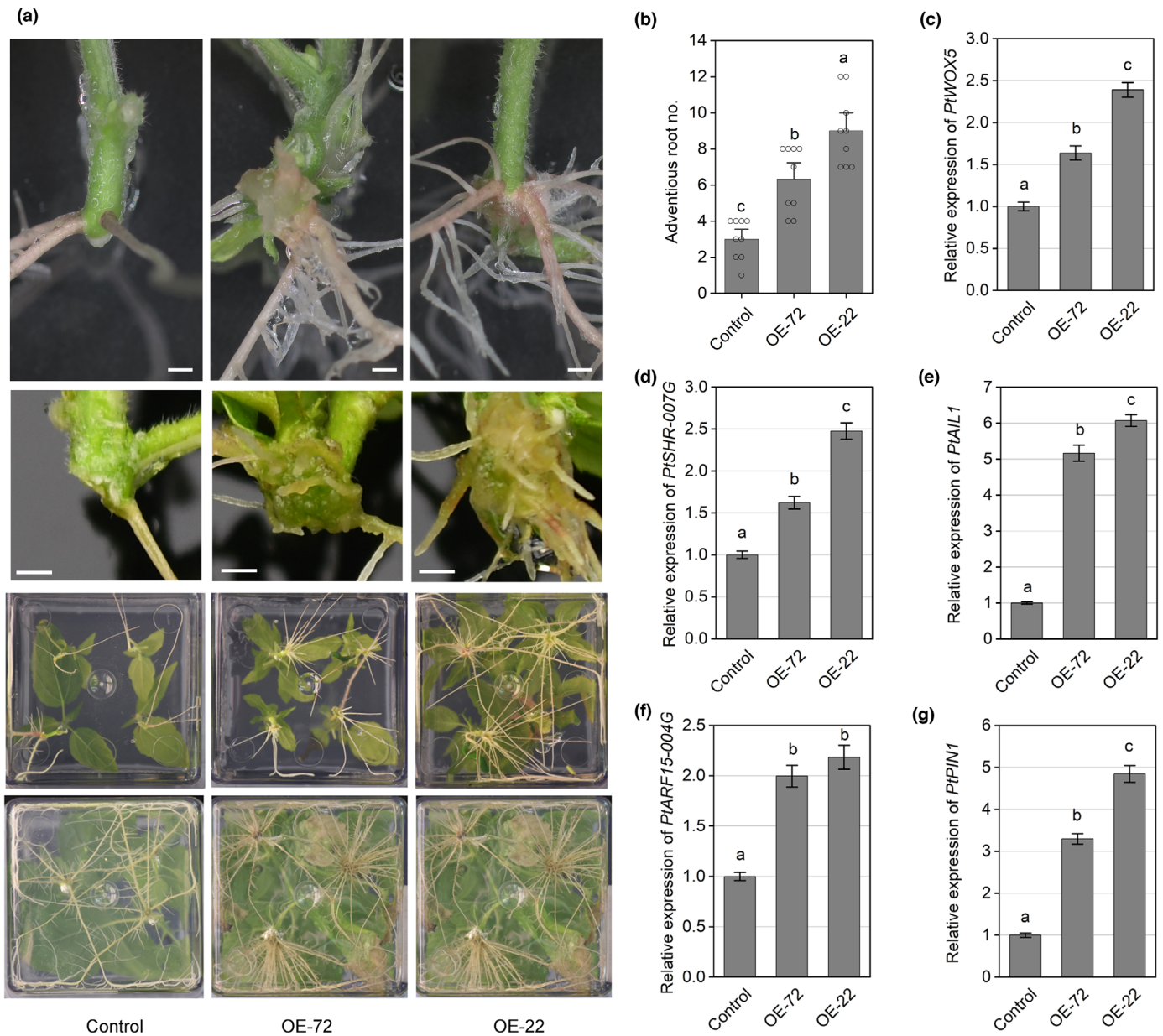
Fig. 4 Overexpression of *PtrXB38* promotes base-born root formation in poplar (*Populus tremula* × *Populus alba*). (a) Morphological phenotypes of the callus and adventitious root regeneration in control and PtrXB38-OE micro-propagated cuttings. Upper two panels show the root formation of 12-d-old plants. Bars, 1 mm. Lower two panels show the root systems of 2- and 4-wk-old plants, respectively. (b) Adventitious root numbers of control and two *PtrXB38-OE* lines. (c–g) Expression of adventitious root-development-related genes *PtWOX5* (c), *PtSHR-007G* (d), *PtAIL1* (e), *PtARF15-004G* (f), and *PtPIN1* (g) in control and *PtrXB38-OE* micro-propagated cuttings. Bar charts represent mean ± SE ($n \geq 3$ independent plants), and different letters represent significant difference between groups ($P \leq 0.05$) determined by one-way ANOVA followed by Tukey's test.

enriched among the DEPs (Fig. S14). These results are consistent with previous eQTL predictions and support the view that *PtrXB38* regulation of root development involves wounding response and auxin signaling. This insight is corroborated by the finding that auxin biosynthesis, signaling pathway, transport, and response-related genes/proteins were highly induced in *PtrXB38-OE* plants from transcriptome and proteome analyses. Notably, ARF proteins were significantly accumulated in the *PtrXB38-OE* root samples (Fig. 5a,b). To further verify the contribution of auxin transport in *PtrXB38*-controlled root development, an auxin transport inhibitor, NPA, was applied during root

formation. We found 5 μM NPA completely blocked root formation in both control and *PtrXB38-OE* micro-cuttings, and the promotive effect of PtrXB38 on AR formation was gradually attenuated or abolished by NPA treatments (Fig. 5c,d). To better evaluate the genotype × treatment effect of *PtrXB38-OE* events under different concentration of NPA treatments, we performed a generalized linear mixed model analysis on the adventitious root number. The results showed that adventitious root numbers of OE-72 and OE-22 are significantly different from control plants at mock conditions, but not at NPA treatment conditions (Table S9). These results suggest that *PtrXB38*-regulated root
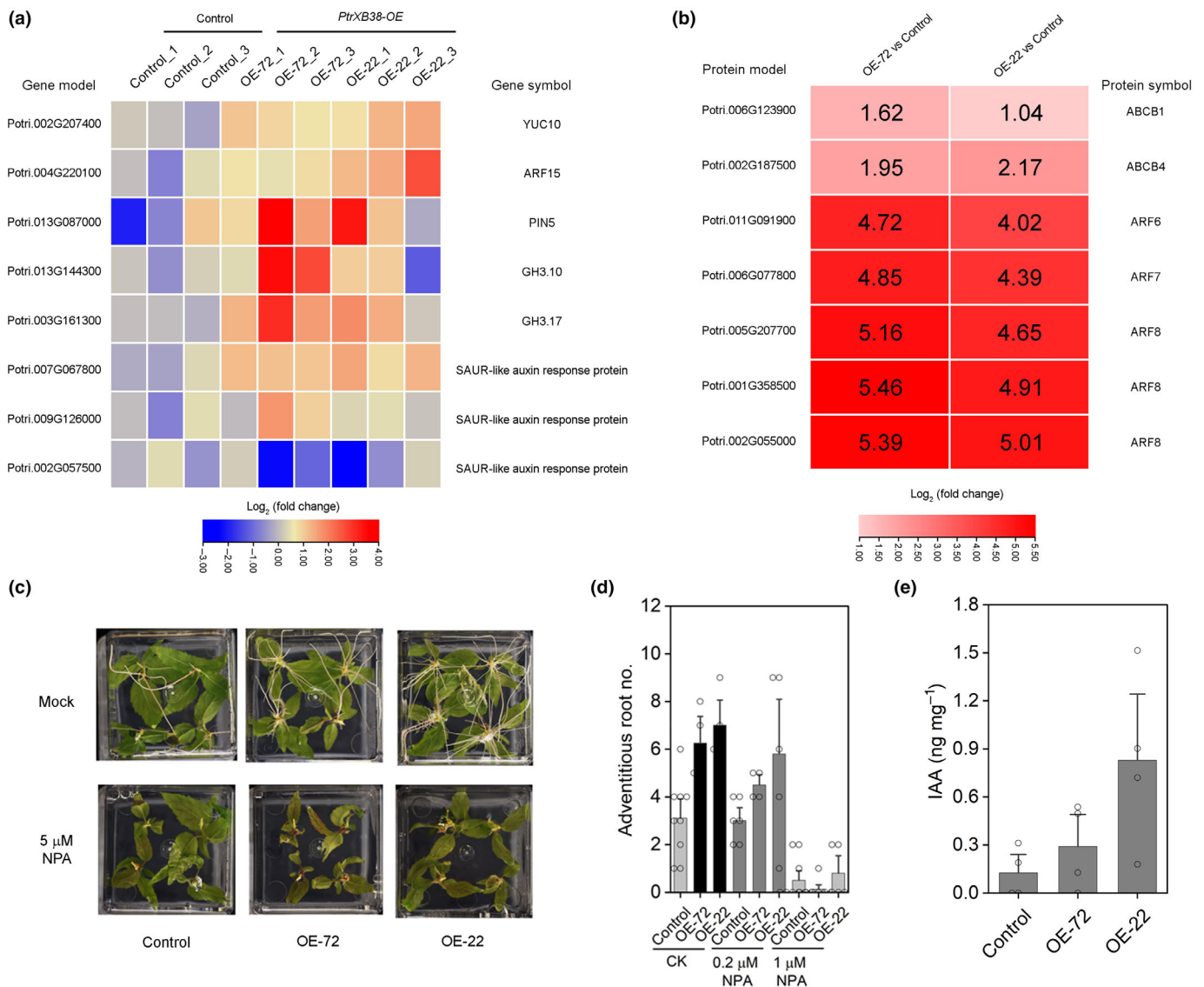
Fig. 5 Auxin signaling and transport is essential for PtrXB38-mediated adventitious root formation in *Populus tremula × Populus alba*. (a) Log-fold changes of transcript levels of auxin biosynthesis, signaling, transport, and response-related genes in 12-d-old root samples of *PtrXB38-OE* vs control plants, based on RNA-seq results. (b) Log-fold changes of protein abundance of auxin response factor in 12-d-old root samples of *PtrXB38-OE* vs control plants, based on quantitative proteomics. (c) Root formation of *PtrXB38-OE* plants upon auxin transport inhibitor treatment. (d) Adventitious root number of *PtrXB38-OE* plants with 0.2 and 1 μM NPA treatments. Bar charts represent mean ± SE ($n \geq 3$ independent plants). (e) IAA contents in the roots of *PtrXB38-OE* plants grown in ½-strength Murashige & Skoog medium. Bar charts represent mean ± SE ($n = 4$ independent plants).

development depends on auxin transport and signaling. Furthermore, since *YUC10* gene expression was upregulated in the roots of *PtrXB38-OE* (Fig. 5a), we measured the content of the major endogenous auxin, IAA. The results show that IAA content is higher in *PtrXB38-OE* plants than in control plants, and this is correlated with the expression levels of *PtrXB38* (Figs 5e, S4).

Gene ontology enrichment analysis for DEPs also identified proteins under the term 'S-adenosylmethionine biosynthetic process', implying that *PtrXB38* may affect ethylene biosynthesis (Fig. S13a). In fact, it has been reported that the E3 ligase XBAT32 specifically mediates ACC synthases (ACS) degradation through the ubiquitin/26S proteome pathway in *Arabidopsis* (Prasad *et al.*, 2010; Druege *et al.*, 2016). However, we did not observe a decreased abundance of ACS proteins in *PtrXB38-OE*

root samples. Instead, we found that the transcript abundance of several genes encoding ethylene biosynthesis-related enzymes, such as SAM synthetase (SAMS) and ACC oxidases (ACOs), were upregulated in *PtrXB38-OE* root samples (Fig. S14a). Likewise, their protein levels were highly accumulated (Fig. S12b). Furthermore, many *ERF* genes were upregulated in *PtrXB38-OE* root samples (Fig. S12a). All these lines of evidence suggest that *PtrXB38* also enhances ethylene biosynthesis and signaling. This inference was supported by the observation that ethylene biosynthesis inhibitor, AVG, inhibited adventitious root formation at high concentrations, and suppressed adventitious root promotion by *PtrXB38-OE* at lower concentrations (Fig. S12c,d,e). Therefore, we concluded that both auxin and ethylene signaling are required for *PtrXB38*-mediated adventitious root

development. Moreover, we found that nitrogen transporter genes, such as *Nitrate transporter 1.7* (*NRT1.7*) and *AMMO-NIUM TRANSPORTER 1;1* (*AMT1;1*), were upregulated in the roots of *PtrXB38-OE* plants, suggesting that PtrXB38 could also increase the nitrogen uptake ability and promote plant growth (Fig. S15).

Subcellular localization, E3 ligase activity, and interacting proteins of PtrXB38

Phenotypic analysis of *PtrXB38-OE* transgenic plants suggests that PtrXB38 is an important regulator of adventitious

development, which was further supported by the studies using auxin transport inhibitor and ethylene biosynthesis inhibitors, and by omics analyses. Both auxin and ethylene regulate root development by affecting the distribution of auxin transporters which associates with the endocytosis pathway including the plasma membrane, Golgi apparatus, and endoplasmic reticulum (ER). Subcellular localization of PtrXB38-GFP was examined by transient expression in *Populus* protoplasts. The results showed that PtrXB38-GFP fusion proteins were detected in the cytosol which co-localized with a Golgi marker. These results suggested that PtrXB38 is localized in Golgi apparatus and may affect the endocytosis pathway (Fig. 6a).
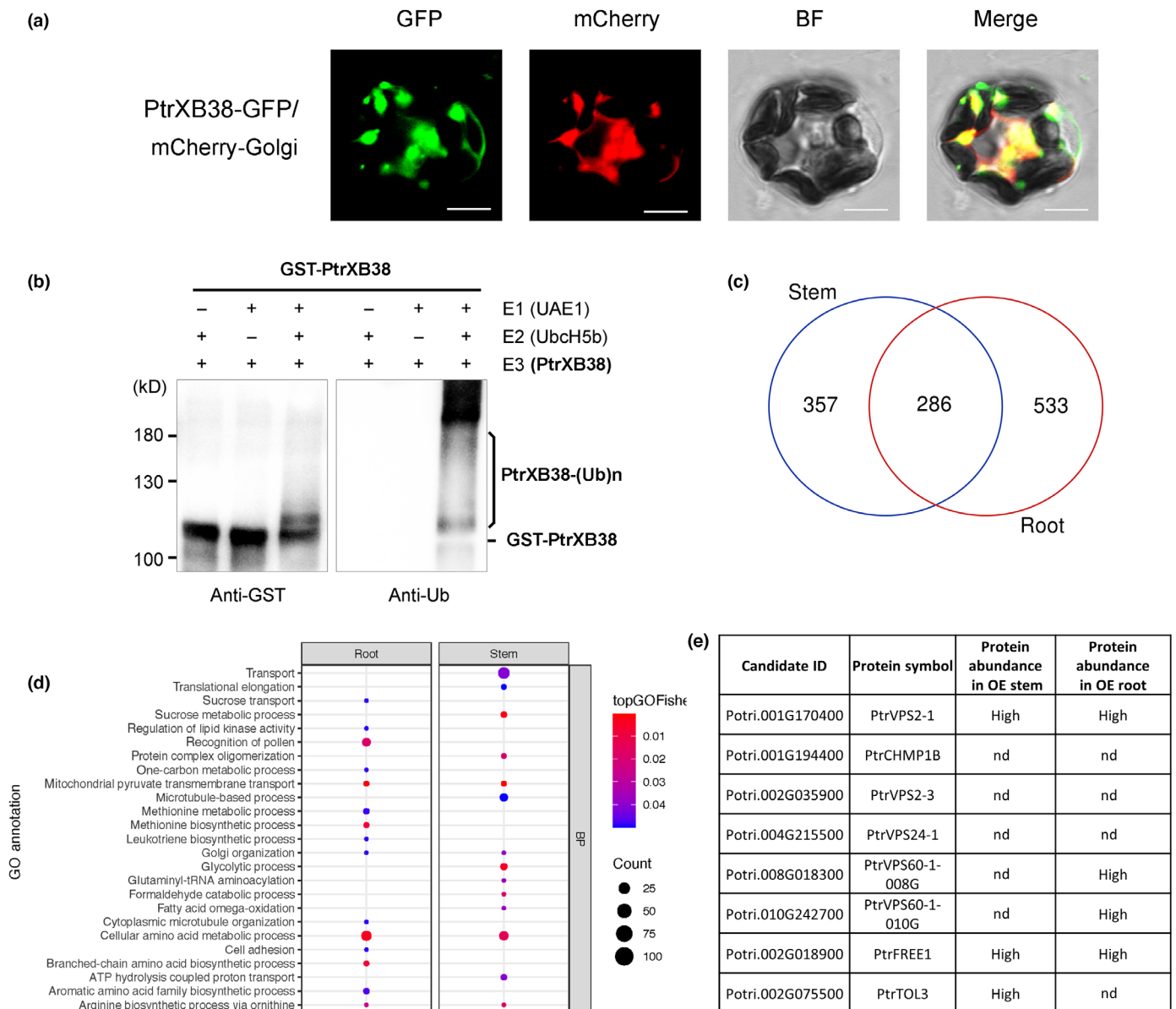

Fig. 6 *PtrXB38* encodes a functional E3 ligase. (a) Subcellular localization of PtrXB38 in the protoplasts of *Populus tremula × Populus alba*. Overlapping of PtrXB38-GFP (green color) and Golgi marker (red color) is indicated as the yellow color. BF, bright field. Bars, 5 μm. (b) Autoubiquitination assay of PtrXB38. The ubiquitination reaction contained 25 ng UAE1 (human E1), 100 ng UbcH5b (E1), 500 ng GST-PtrXB38, and 8 μg Ubiquitin. After the reaction, polyubiquitinated PtrXB38 was analyzed by western blot using anti-GST or anti-Ub antibodies. (c) Venn diagram of PtrXB38-interacting proteins identified in stem and root tissues. (d) GO annotation of PtrXB38-interacting proteins. (e) ESCRT subunits identified as the PtrXB38-interacting proteins. 'High' indicates that the protein abundance is highly accumulated in *PtrXB38-OE* stem or root samples compared to the control plants. nd, nondetectable.

Because PtrXB38 is predicted to be an E3 ligase, we wanted to evaluate whether PtrXB38 indeed possesses E3 ligase activity. When incubated with ubiquitin activating enzyme (E1) and ubiquitin conjugating enzyme (E2), PtrXB38 showed strong ubiquitination activity (Fig. 6b), suggesting that PtrXB38 is a functional E3 ligase which may target its interacting proteins for ubiquitination.

Subsequently, we performed GST-PtrXB38 pull-down followed by mass spectrometry to identify PtrXB38-interacting proteins in total protein extracts from stem or root tissue. We identified 643 and 819 potential interacting proteins in stem and root tissues, respectively (Fig. 6c; Tables S10, S11), among which are proteins that are categorized as protein transport, Golgi organization, and metabolic process (Fig. 6d). The ESCRT complexes are required for multivesicular body-based endosomal sorting of integral membrane proteins, such as PIN2 (Gao et al., 2017). Interestingly, our pull-down/MS analysis identified eight subunits of the ESCRT machinery: one ESCRT-0 component TOM1-like 3 (TOL3), six ESCRT-III components, and one plant unique ESCRT component FYVE domain protein required for endosomal sorting 1 (FREE1), as PtrXB38-interacting proteins (Fig. 6e). Among them, a subset of proteins showed varying level of abundance in PtrXB38-OE plants compared to the control plants (Fig. 6e). BiFC assays validated in vivo interactions between PtrXBAT38 and ESCRT subunits, which can be direct or associated within protein complexes (Figs 7b, S16). GST pull-down experiments further confirm the physical protein–protein interactions of PtrXB38 with PtrTOL3 and PtrVPS24 (Fig. 7a). These results suggest that the developmental regulator PtrTOL3 is a strong candidate as a substrate of PtrXB38. Further studies are needed to unravel the regulatory mechanism and biological significance of these protein interactions.

Discussion

In this study, we identified the *PtrXB38* locus as an eQTL hotspot that affected the expression of > 500 of genes in *trans* (Fig. 1). Although we describe PtrXB38 as an important regulator of adventitious root development, considering its hierarchical position within the predicted regulatory networks, PtrXB38 may play a key role in multiple other biological processes in leaves and xylem tissues. Considering no phenotypic differences were observed in *PtrXB38-KO* plants, we hypothesize that this is likely due to the potential genetic redundancy among members of the *PtrXB3* gene family, as there are nine members in *Populus* (Figs S1, S2) and one of them, PtrXB32 (Potri.018G098400), has previously been reported to be involved in root development (Trupiano et al., 2013). Noticeably, although *PtrXB38* belongs to a multi-member *PtrXB3* gene family, we did not identify other *PtrXB3* gene loci, which suggests that *PtrXB38* might be a major eQTL hotspot while other *PtrXB3* genes may have minor effects in regulating gene expression. Lastly, the eQTL regulatory network suggests that *PtrXB38* participates in regulating root development. However, we were not able to recognize the alleles/accessions that have positive or negative effects on adventitious root development. On the other hand, a recent GWAS study has identified 277 associations of *P. trichocarpa* accession with adventitious root development and discovered many developmental regulators (Nagle et al., 2022). Integration of eQTL and GWAS data may help reveal the genetic mechanisms of adventitious root development in *Populus*.

Auxin plays central roles in plant root development. It has been reported that an auxin/ARF/LBD regulatory module mediates callus formation and lateral root formation (Fan et al., 2012). Stem-born root formation is also regulated by LBD and auxin response (Omary et al., 2022). Our genome-wide transcriptomics and proteomics analyses revealed that overexpression of *PtrXB38* can enhance auxin response, impacting the signaling pathway and transport of auxin in the stem and root tissues of poplar (Figs 3, 5). In addition, PtrXB38 increased auxin contents in the roots of the *PtrXB38-OE* plants, which may lead to the enhanced callus and adventitious root formation (Fig. 3). Noticeably, callus formation can also impede the formation of base-born roots because it delays the formation of the adventitious roots, and the calli may not develop new roots as well (Singh & Ansari, 2014). It will be of interest to study how PtrXB38 simultaneously promotes callus and adventitious root formation.

Ethylene is another plant hormone that participates in plant root development. Both XBAT32 and its ortholog of PtrXB32 in *Populus* have also been reported to control lateral root formation (Nodzon et al., 2004; Prasad et al., 2010; Trupiano et al., 2013).
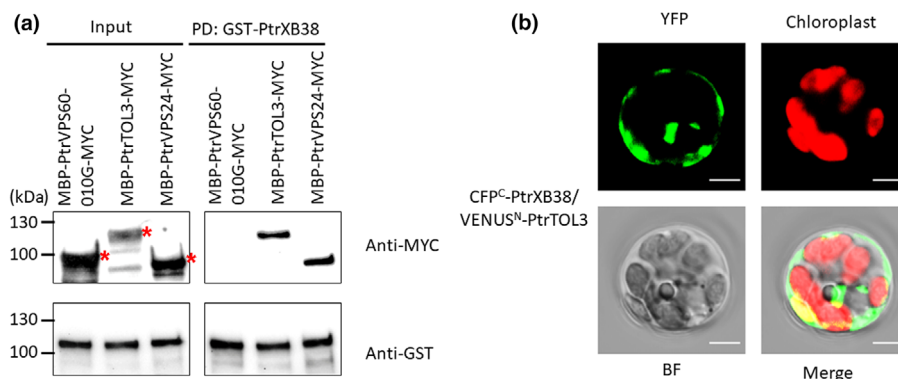

Fig. 7 Interaction of PtrXB38 with PtrTOL3 *in vitro* and *in vivo*. (a) *In vitro* pull-down assay of PtrXB38 with PtrVPS60-010G, PtrTOL3, and PtrVPS24. Asterisks (*) indicate the expected position of the recombinant proteins. (b) Bimolecular fluorescence complementation (BiFC) assay of PtrXB38 with PtrTOL3 the protoplasts of *Populus tremula* × *Populus alba*. YFP signals were detected when CFP^C-PtrXB38 co-transfected with VENUS^N-PtrTOL3. Bars, 5 µm.

Furthermore, XBAT32 increases lateral root formation in *Arabidopsis* by repressing ethylene biosynthesis (Prasad *et al.*, 2010). Although XBAT35 has not been reported to regulate root development, it negatively regulates ethylene-mediated apical hook curvature (Carvalho *et al.*, 2012). Different from XBAT32, overexpression of PtrXB38 increases the protein abundances of SAMS and ACO enzymes (Fig. S12b). Root development in *PtrXB38-OE* plants was attenuated when inhibiting ethylene production, suggesting that ethylene contributes to PtrXB38-mediated adventitious root development in *Populus* (Fig. S12d,e). It is known that auxin and ethylene regulate each other's biosynthesis and signaling (Muday *et al.*, 2012; Qin & Huang, 2018), but it remains elusive whether it is the biosynthesis and signaling of auxin or ethylene that is directly regulated by *PtrXB38*. Future studies on identification of *PtrXB38* direct targets may provide answers to this question. Interestingly, neither the *XBAT35-OE* nor the *xbat35* null mutant in *Arabidopsis* showed differences in root development, indicative of a potential functional diversity of XBAT35 in herbaceous and PtrXB38 woody species (Carvalho *et al.*, 2012).

In *Arabidopsis*, the two splice variants, *XBAT35.1* and *XBAT35.2*, encode two isoforms of XBAT35 localized in different subcellular compartments. Accordingly, the functions of these two proteins are different. For example, transient expression of XBAT35.2 rather than XBAT35.1 triggered cell death in tobacco leaves (Carvalho *et al.*, 2012; Liu *et al.*, 2017). There are two splicing forms annotated in *P. trichocarpa* v.3.1 reference genome. However, these two splicing forms only showed differences in the 3′ UTR region and thus do not change the CDS or amino acid sequences. Similar to XBAT35.2, PtrXB38 (Potri.010G070800.6) lacks a nuclear localization signal and was found localized in the Golgi apparatus. Recent reports showed that XBAT35.2 regulates protein trafficking between endosome and vacuole by mediating protein degradation of VPS23A, an ESCRT-I component (Yu *et al.*, 2020; Liu *et al.*, 2022). Coincidently, our proteomics and IP-MS studies identified eight subunits of the ESCRT complex, and some of them are required for normal auxin transport and plant development (Fig. 6). For example, mutations of ESCRT components, TOL3, FREE1, CHMP1B, VPS28A, and VPS28B, showed abnormal expression pattern of *PINs* and alternation of auxin-mediated plant development, including root development, in *Arabidopsis* (Korbei *et al.*, 2013; Gao *et al.*, 2014; Liu *et al.*, 2020). Since these ESCRT components have been reported to directly affect the plasma membrane asymmetrical localization of PIN proteins and intercellular polar auxin transport (Gao *et al.*, 2014, 2017), we speculate that PtrXB38 regulates root development by influencing auxin transport via interacting with and modifying the stability of proteins in the ESCRT machinery.

Recent advances revealed that phytohormone signaling contributes to shaping plant root system architecture in both agronomic crops and bioenergy woody species (Csukasi *et al.*, 2009; Depuydt & Hardtke, 2011). Here, we report that the E3 ligase gene, *PtrXB38*, identified as a potential master regulator by eQTL mapping, regulates stem-born and base-born adventitious root formation and development in poplar. We further demonstrate that the effects of PtrXB38 in root development are dependent on auxin and ethylene signaling pathways. Our work showcases the power of population-wide eQTL mapping, followed by reverse genetics validation, for discovering novel plant development regulators in woody plants (Muchero *et al.*, 2018; Zhang *et al.*, 2018; Labbé *et al.*, 2019).

Competing interests

None declared.

Author contributions

ORCID

Paul E. Abraham (ID) https://orcid.org/0000-0003-2685-9123
Jin-Gui Chen (ID) https://orcid.org/0000-0002-1752-4201
Wellington Muchero (ID) https://orcid.org/0000-0002-0200-9856
Chung-Jui Tsai (ID) https://orcid.org/0000-0002-9282-7704
Tao Yao (ID) https://orcid.org/0000-0002-9382-0731
Larry M. York (ID) https://orcid.org/0000-0002-1995-9479
Jin Zhang (ID) https://orcid.org/0000-0002-8397-5078

Data availability

The raw reads have been deposited at the SRA and can be accessed with the BioProject ID PRJNA785328.

References

Alexa A, Rahnenführer J, Lengauer T. 2006. Improved scoring of functional groups from gene expression data by decorrelating GO graph structure. *Bioinformatics* 22: 1600–1607.

Babicki S, Arndt D, Marcu A, Liang Y, Grant JR, Maciejewski A, Wishart DS. 2016. Heatmapper: web-enabled heat mapping for all. *Nucleic Acids Research* 44: W147–W153.

Balmant KM, Noble JD, Alves FC, Dervinis C, Conde D, Schmidt HW, Vazquez AI, Barbazuk WB, Campos GL, Resende MFR Jr et al. 2020. Xylem systems genetics analysis reveals a key regulator of lignin biosynthesis in *Populus deltoides*. *Genome Research* 30: 1131–1143.

Bannoud F, Bellini C. 2021. Adventitious rooting in *Populus* species: update and perspectives. *Frontiers in Plant Science* 12: 668837.

Bellini C, Pacurar DI, Perrone I. 2014. Adventitious roots and lateral roots: similarities and differences. *Annual Review of Plant Biology* 65: 639–666.

Bewg WP, Harding SA, Engle NL, Vaidya BN, Zhou R, Reeves J, Horn TW, Joshee N, Jenkins JW, Shu S et al. 2022. Multiplex knockout of trichome-regulating MYB duplicates in hybrid poplar using a single gRNA. *Plant Physiology* 189: 516–526.

Cai H, Yang C, Liu S, Qi H, Wu L, Xu L-A, Xu M. 2019. MiRNA-target pairs regulate adventitious rooting in *Populus*: a functional role for miR167a and its target auxin response factor 8. *Tree Physiology* 39: 1922–1936.

Carvalho SD, Saraiva R, Maia TM, Abreu IA, Duque P. 2012. XBAT35, a novel Arabidopsis RING E3 ligase exhibiting dual targeting of its splice isoforms, is involved in ethylene-mediated regulation of apical hook curvature. *Molecular Plant* 5: 1295–1309.

Chen C, Chen H, Zhang Y, Thomas HR, Frank MH, He Y, Xia R. 2020. TBTOOLS: an integrative toolkit developed for interactive analyses of big biological data. *Molecular Plant* 13: 1194–1202.

Cheng SLH, Wu H-W, Xu H, Singh RM, Yao T, Jang I-C, Chua N-H. 2022. Nutrient status regulates MED19a phase separation for ORESARA1-dependent senescence. *New Phytologist* 236: 1779–1795.

Csukasi F, Merchante C, Valpuesta V. 2009. Modification of plant hormone levels and signaling as a tool in plant biotechnology. *Biotechnology Journal* 4: 1293–1304.

Cubillos FA, Coustham V, Loudet O. 2012. Lessons from eQTL mapping studies: non-coding regions and their role behind natural phenotypic variation in plants. *Current Opinion in Plant Biology* 15: 192–198.

Depuydt S, Hardtke CS. 2011. Hormone signalling crosstalk in plant growth regulation. *Current Biology* 21: R365–R373.

Díaz-Sala C. 2020. A perspective on adventitious root formation in tree species. *Plants* 9: 1789.

Dobin A, Davis CA, Schlesinger F, Drenkow J, Zaleski C, Jha S, Batut P, Chaisson M, Gingeras TR. 2013. STAR: ultrafast universal RNA-seq aligner. *Bioinformatics* 29: 15–21.

Domagalska MA, Leyser O. 2011. Signal integration in the control of shoot branching. *Nature Reviews Molecular Cell Biology* 12: 211–221.

Drost DR, Benedict CI, Berg A, Novaes E, Novaes CRDB, Yu Q, Dervinis C, Maia JM, Yap J, Miles B et al. 2010. Diversification in the genetic architecture of gene expression and transcriptional networks in organ differentiation of *Populus*. *Proceedings of the National Academy of Sciences, USA* 107: 8492–8497.

Druege U, Franken P, Hajirezaei MR. 2016. Plant hormone homeostasis, signaling, and function during adventitious root formation in cuttings. *Frontiers in Plant Science* 7: 381.

Eng JK, McCormack AL, Yates JR. 1994. An approach to correlate tandem mass spectral data of peptides with amino acid sequences in a protein database. *Journal of the American Society for Mass Spectrometry* 5: 976–989.

Fan M, Xu C, Xu K, Hu Y. 2012. LATERAL ORGAN BOUNDARIES DOMAIN transcription factors direct callus formation in Arabidopsis regeneration. *Cell Research* 22: 1169–1180.

Gao C, Luo M, Zhao Q, Yang R, Cui Y, Zeng Y, Xia J, Jiang L. 2014. A unique plant ESCRT component, FREE1, regulates multivesicular body protein sorting and plant growth. *Current Biology* 24: 2556–2563.

Gao C, Zhuang X, Shen J, Jiang L. 2017. Plant ESCRT complexes: moving beyond endosomal sorting. *Trends in Plant Science* 22: 986–998.

Geisler M, Aryal B, di Donato M, Hao P. 2017. A critical view on ABC transporters and their interacting partners in auxin transport. *Plant and Cell Physiology* 58: 1601–1614.

ten Hove CA, Willemsen V, de Vries WJ, van Dijken A, Scheres B, Heidstra R. 2010. SCHIZORIZA encodes a nuclear factor regulating asymmetry of stem cell divisions in the Arabidopsis root. *Current Biology* 20: 452–457.

Jacobs TB, LaFayette PR, Schmitz RJ, Parrott WA. 2015. Targeted genome modifications in soybean with CRISPR/Cas9. *BMC Biotechnology* 15: 16.

Jiang L, He L, Fountoulakis M. 2004. Comparison of protein precipitation methods for sample preparation prior to proteomic analysis. *Journal of Chromatography A* 1023: 317–320.

Käll L, Canterbury JD, Weston J, Noble WS, MacCoss MJ. 2007. Semi-supervised learning for peptide identification from shotgun proteomics datasets. *Nature Methods* 4: 923–925.

Kleine-Vehn J, Friml J. 2008. Polar targeting and endocytic recycling in auxin-dependent plant development. *Annual Review of Cell and Developmental Biology* 24: 447–473.

Koncz C, Schell J. 1986. The promoter of TL-DNA gene 5 controls the tissue-specific expression of chimaeric genes carried by a novel type of *Agrobacterium* binary vector. *Molecular and General Genetics* 204: 383–396.

Korbei B, Moulinier-Anzola J, De-Araujo L, Lucyshyn D, Retzer K, Khan Muhammad A, Luschnig C. 2013. Arabidopsis TOL proteins act as gatekeepers for vacuolar sorting of PIN2 plasma membrane protein. *Current Biology* 23: 2500–2505.

Krzywinski M, Schein J, Birol I, Connors J, Gascoyne R, Horsman D, Jones SJ, Marra MA. 2009. CIRCOS: an information aesthetic for comparative genomics. *Genome Research* 19: 1639–1645.

Kumar S, Stecher G, Li M, Knyaz C, Tamura K. 2018. MEGA X: molecular evolutionary genetics analysis across computing platforms. *Molecular Biology and Evolution* 35: 1547–1549.

Labbé J, Muchero W, Czarnecki O, Wang J, Wang X, Bryan AC, Zheng K, Yang Y, Xie M, Zhang J et al. 2019. Mediation of plant-mycorrhizal interaction by a lectin receptor-like kinase. *Nature Plants* 5: 676–680.

Lakehal A, Bellini C. 2019. Control of adventitious root formation: insights into synergistic and antagonistic hormonal interactions. *Physiologia Plantarum* **165**: 90–100.

Lenz RR, Shrestha HK, Carrell AA, Labbé J, Hettich RL, Abraham PE, LeBoldus JM. 2022. Proteomics reveals pathways linked to septoria canker resistance and susceptibility in *Populus trichocarpa*. *Frontiers in Analytical Science* **2**: 1020111.

Letunic I, Khedkar S, Bork P. 2020. SMART: recent updates, new developments and status in 2020. *Nucleic Acids Research* **49**: D458–D460.

Li C, Potuschak T, Colón-Carmona A, Gutiérrez RA, Doerner P. 2005. Arabidopsis TCP20 links regulation of growth and cell division control pathways. *Proceedings of the National Academy of Sciences, USA* **102**: 12978–12983.

Li J, Zhang J, Jia H, Liu B, Sun P, Hu J, Wang L, Lu M. 2017. The WUSCHEL-related homeobox 5a (PtoWOX5a) is involved in adventitious root development in poplar. *Tree Physiology* **38**: 139–153.

Li Q, Serio RJ, Schofield A, Liu H, Rasmussen SR, Hofius D, Stone SL. 2020. Arabidopsis RING-type E3 ubiquitin ligase XBAT35.2 promotes proteasome-dependent degradation of ACD11 to attenuate abiotic stress tolerance. *The Plant Journal* **104**: 1712–1723.

Liu G, Liang J, Lou L, Tian M, Zhang X, Liu L, Zhao Q, Xia R, Wu Y, Xie Q *et al.* 2022. The deubiquitinases UBP12 and UBP13 integrate with the E3 ubiquitin ligase XBAT35.2 to modulate VPS23A stability in ABA signaling. *Science Advances* **8**: eabl5765.

Liu H, Ravichandran S, Teh O-k, McVey S, Lilley C, Teresinski HJ, Gonzalez-Ferrer C, Mullen RT, Hofius D, Prithiviraj B *et al.* 2017. The RING-type E3 ligase XBAT35.2 is involved in cell death induction and pathogen response. *Plant Physiology* **175**: 1469–1483.

Liu J, Wang Y, Cheng Y. 2020. The ESCRT-I components VPS28A and VPS28B are essential for auxin-mediated plant development. *The Plant Journal* **104**: 1617–1634.

Livak KJ, Schmittgen TD. 2001. Analysis of relative gene expression data using real-time quantitative PCR and the 2(-Delta Delta C(T)) method. *Methods* **25**: 402–408.

Love MI, Huber W, Anders S. 2014. Moderated estimation of fold change and dispersion for RNA-seq data with DESEQ2. *Genome Biology* **15**: 550.

Mistry J, Chuguransky S, Williams L, Qureshi M, Salazar Gustavo A, Sonnhammer ELL, Tosatto SCE, Paladin L, Raj S, Richardson LJ *et al.* 2020. PFAM: the protein families database in 2021. *Nucleic Acids Research* **49**: D412–D419.

Moulinier-Anzola J, Schwihla M, De-Araújo L, Artner C, Jörg L, Konstantinova N, Luschnig C, Korbei B. 2020. TOLs function as ubiquitin receptors in the early steps of the ESCRT pathway in higher plants. *Molecular Plant* **13**: 717–731.

Muchero W, Sondreli KL, Chen J-G, Urbanowicz BR, Zhang J, Singan V, Yang Y, Brueggeman RS, Franco-Coronado J, Abraham N *et al.* 2018. Association mapping, transcriptomics, and transient expression identify candidate genes mediating plant–pathogen interactions in a tree. *Proceedings of the National Academy of Sciences, USA* **115**: 11573–11578.

Muday GK, Rahman A, Binder BM. 2012. Auxin and ethylene: collaborators or competitors? *Trends in Plant Science* **17**: 181–195.

Müller M, Munné-Bosch S. 2011. Rapid and sensitive hormonal profiling of complex plant samples by liquid chromatography coupled to electrospray ionization tandem mass spectrometry. *Plant Methods* **7**: 37.

Nagle MF, Yuan J, Kaur D, Ma C, Peremyslova E, Jiang Y, Willig CJ, Goralogia GS, de Rivera AN, McEldowney M *et al.* 2022. GWAS identifies candidate genes controlling adventitious rooting in *Populus trichocarpa*. *bioRxiv*. doi: 10.1101/2022.06.14.496209.

Nelson BK, Cai X, Nebenführ A. 2007. A multicolored set of *in vivo* organelle markers for co-localization studies in Arabidopsis and other plants. *The Plant Journal* **51**: 1126–1136.

Nodzon LA, Xu WH, Wang Y, Pi LY, Chakrabarty PK, Song WY. 2004. The ubiquitin ligase XBAT32 regulates lateral root development in Arabidopsis. *The Plant Journal* **40**: 996–1006.

Omary M, Gil-Yarom N, Yahav C, Steiner E, Hendelman A, Efroni I. 2022. A conserved superlocus regulates above- and belowground root initiation. *Science* **375**: eabf4368.

Pan X, Welti R, Wang X. 2010. Quantitative analysis of major plant hormones in crude plant extracts by high-performance liquid chromatography-mass spectrometry. *Nature Protocols* **5**: 986–992.

Park BS, Yao T, Seo JS, Wong ECC, Mitsuda N, Huang CH, Chua NH. 2018. Arabidopsis NITROGEN LIMITATION ADAPTATION regulates ORE1 homeostasis during senescence induced by nitrogen deficiency. *Nature Plants* **4**: 898–903.

Petrášek J, Friml J. 2009. Auxin transport routes in plant development. *Development* **136**: 2675–2688.

Prasad ME, Schofield A, Lyzenga W, Liu H, Stone SL. 2010. Arabidopsis RING E3 ligase XBAT32 regulates lateral root production through its role in ethylene biosynthesis. *Plant Physiology* **153**: 1587–1596.

Qin H, Huang R. 2018. Auxin controlled by ethylene steers root development. *International Journal of Molecular Sciences* **19**: 3656.

Ramirez-Parra E, Perianez-Rodriguez J, Navarro-Neila S, Gude I, Moreno-Risueno MA, del Pozo JC. 2017. The transcription factor OBP4 controls root growth and promotes callus formation. *New Phytologist* **213**: 1787–1801.

Rigal A, Yordanov YS, Perrone I, Karlberg A, Tisserant E, Bellini C, Busov VB, Martin F, Kohler A, Bhalerao R *et al.* 2012. The AINTEGUMENTA LIKE1 homeotic transcription factor PtAIL1 controls the formation of adventitious root primordia in poplar. *Plant Physiology* **160**: 1996–2006.

Shrestha H, Yao T, Qiao Z, Muchero W, Hettich RL, Chen J-G, Abraham PE. 2023. Lectin receptor-like kinase signaling during engineered ectomycorrhiza colonization. *Cell* **12**: 1082.

Singh S, Ansari S. 2014. Callus formation impedes adventitious rhizogenesis in air layers of broadleaved tree species. *Annals of Forest Research* **57**: 47–54.

Steffens B, Rasmussen A. 2015. The physiology of adventitious roots. *Plant Physiology* **170**: 603–617.

Subramanian B, Gao S, Lercher MJ, Hu S, Chen WH. 2019. EVOLVIEW v.3: a webserver for visualization, annotation, and management of phylogenetic trees. *Nucleic Acids Research* **47**: W270–W275.

Trupiano D, Yordanov Y, Regan S, Meilan R, Tschaplinski T, Scippa GS, Busov V. 2013. Identification, characterization of an AP2/ERF transcription factor that promotes adventitious, lateral root formation in *Populus*. *Planta* **238**: 271–282.

Tuskan GA, Difazio S, Jansson S, Bohlmann J, Grigoriev I, Hellsten U, Putnam N, Ralph S, Rombauts S, Salamov A *et al.* 2006. The genome of black cottonwood, *Populus trichocarpa* (Torr. & Gray). *Science* **313**: 1596–1604.

Tyanova S, Temu T, Sinitcyn P, Carlson A, Hein MY, Geiger T, Mann M, Cox J. 2016. The PERSEUS computational platform for comprehensive analysis of (prote)omics data. *Nature Methods* **13**: 731–740.

Wade AR, Duruflé H, Sanchez L, Segura V. 2022. eQTLs are key players in the integration of genomic and transcriptomic data for phenotype prediction. *BMC Genomics* **23**: 476.

Wang J, Carper DL, Burdick LH, Shrestha HK, Appidi MR, Abraham PE, Timm CM, Hettich RL, Pelletier DA, Doktycz MJ. 2021. Formation, characterization and modeling of emergent synthetic microbial communities. *Computational and Structural Biotechnology Journal* **19**: 1917–1927.

Wang YS, Pi LY, Chen X, Chakrabarty PK, Jiang J, De Leon AL, Liu GZ, Li L, Benny U, Oard J *et al.* 2006. Rice XA21 binding protein 3 is a ubiquitin ligase required for full Xa21-mediated disease resistance. *Plant Cell* **18**: 3635–3646.

Xiao L, Du Q, Fang Y, Quan M, Lu W, Wang D, Si J, El-Kassaby YA, Zhang D. 2021. Genetic architecture of the metabolic pathway of salicylic acid biosynthesis in *Populus*. *Tree Physiology* **41**: 2198–2215.

Xie C, Mao X, Huang J, Ding Y, Wu J, Dong S, Kong L, Gao G, Li CY, Wei L. 2011. KOBAS 2.0: a web server for annotation and identification of enriched pathways and diseases. *Nucleic Acids Research* **39**(Suppl 2): W316–W322.

Xu C, Tao Y, Fu X, Guo L, Xing H, Li C, Yang Z, Su H, Wang X, Hu J *et al.* 2021. The microRNA476a-RFL module regulates adventitious root formation through a mitochondria-dependent pathway in *Populus*. *New Phytologist* **230**: 2011–2028.

Xu M, Xie W, Huang M. 2015. Two WUSCHEL-related HOMEOBOX genes, PeWOX11a and PeWOX11b, are involved in adventitious root formation of poplar. *Physiologia Plantarum* **155**: 446–456.

Xuan L, Xu M, Chen C, Xu M, Huang M. 2014. Identification and characterization of three PeSHRs and one PeSCR involved in adventitious root development of *Populus*. *Plant Cell, Tissue and Organ Culture (PCTOC)* **117**: 253–264.

Xue LJ, Tsai CJ. 2015. AGESEQ: analysis of genome editing by sequencing. *Molecular Plant* **8**: 1428–1430.

Yates TB, Feng K, Zhang J, Singan V, Jawdy SS, Gunter LE, Ranjan P, Abraham PE, Barry K, Lipzen A *et al.* 2021. The ancient Salicoid genome duplication event: a platform for reconstruction of *de novo* gene evolution in *Populus trichocarpa*. *Genome Biology and Evolution* 13: evab198.

Yu F, Cao X, Liu G, Wang Q, Xia R, Zhang X, Xie Q. 2020. ESCRT-I component VPS23A is targeted by E3 ubiquitin ligase XBAT35 for proteasome-mediated degradation in modulating ABA signaling. *Molecular Plant* 13: 1556–1569.

Yuan X, Zhang S, Liu S, Yu M, Su H, Shu H, Li X. 2013. Global analysis of ankyrin repeat domain C3HC4-type RING finger gene family in plants. *PLoS ONE* 8: e58003.

Yue J, Yang H, Yang S, Wang J. 2020. TDIF regulates auxin accumulation and modulates auxin sensitivity to enhance both adventitious root and lateral root formation in poplar trees. *Tree Physiology* 40: 1534–1547.

Zhang J, Eswaran G, Alonso-Serra J, Kucukoglu M, Xiang J, Yang W, Elo A, Nieminen K, Damen T, Joung JG *et al.* 2019. Transcriptional regulatory framework for vascular cambium development in Arabidopsis roots. *Nature Plants* 5: 1033–1042.

Zhang J, Xie M, Li M, Ding J, Pu Y, Bryan AC, Rottmann W, Winkeler KA, Collins CM, Singan V *et al.* 2020. Overexpression of a Prefoldin beta subunit gene reduces biomass recalcitrance in the bioenergy crop *Populus*. *Plant Biotechnology Journal* 18: 859–871.

Zhang J, Yang Y, Zheng K, Xie M, Feng K, Jawdy SS, Gunter LE, Ranjan P, Singan VR, Engle N *et al.* 2018. Genome-wide association studies and expression-based quantitative trait loci analyses reveal roles of HCT2 in caffeoylquinic acid biosynthesis and its regulation by defense-responsive transcription factors in *Populus*. *New Phytologist* 220: 502–516.

Zhang L, Lu D, Ge X, Du J, Wen S, Xiang X, Du C, Zhou X, Hu J. 2023. Insight into growth and wood properties based on QTL and eQTL mapping in *Populus deltoides* 'Danhong' × *Populus simonii* 'Tongliao1'. *Industrial Crops and Products* 199: 116731.

Zhang LL, Li W, Tian YY, Davis SJ, Liu JX. 2021a. The E3 ligase XBAT35 mediates thermoresponsive hypocotyl growth by targeting ELF3 for degradation in Arabidopsis. *Journal of Integrative Plant Biology* 63: 1097–1103.

Zhang LL, Shao YJ, Ding L, Wang MJ, Davis SJ, Liu JX. 2021b. XBAT31 regulates thermoresponsive hypocotyl growth through mediating degradation of the thermosensor ELF3 in Arabidopsis. *Science Advances* 7: eabf4427.

Zhou X, Stephens M. 2012. Genome-wide efficient mixed-model analysis for association studies. *Nature Genetics* 44: 821–824.

Supporting Information

Additional Supporting Information may be found online in the Supporting Information section at the end of the article.

Fig. S1 Identification of *PtrXB38* as a hotspot by eQTL mapping in *Populus trichocarpa*.

Fig. S2 Phylogenetic tree of XB3 family.

Fig. S3 Protein domains and tissue expression patterns of *PtrXB3* genes.

Fig. S4 Expression levels of *PtrXB38* in independent lines of *PtrXB38-OE* transgenic plants in *Populus tremula* × *Populus alba*.

Fig. S5 Callus formation on the stems of *PtrXB38-OE* plants in *Populus tremula* × *Populus alba*.

Fig. S6 Overexpression of *PtrXB38* alters the transcriptomes of stem and leaf in *Populus tremula* × *Populus alba*.

Fig. S7 Overexpression of *PtrXB38* alters the proteome of stem in *Populus tremula* × *Populus alba*.

Fig. S8 Adventitious root numbers of *PtrXB38-KO* plants in *Populus tremula* × *Populus alba*.

Fig. S9 Overexpression of *PtrXB38* alters the transcriptome of root in *Populus tremula* × *Populus alba*.

Fig. S10 Overexpression of *PtrXB38* alters the proteome of root in *Populus tremula* × *Populus alba*.

Fig. S11 Expression of transcription factor family genes regulated by PtrXB38 in *Populus tremula* × *Populus alba*.

Fig. S12 PtrXB38-regulated adventitious root development involves ethylene biosynthesis and signaling in *Populus tremula* × *Populus alba*.

Fig. S13 Functional category enrichment of the DEGs.

Fig. S14 Functional category enrichment of the DEPs.

Fig. S15 Growth advantage of *PtrXB38-OE* plants in *Populus tremula* × *Populus alba*.

Fig. S16 Interaction of PtrXB38 with ESCRT subunits in the protoplasts of *Populus tremula* × *Populus alba*.

Table S1 List of used primers.

Table S2 eQTL target genes of PtrXB38 hotspot in *Populus trichocarpa*.

Table S3 Transcription factor coding genes among PtrXB38 eQTL targets in *Populus trichocarpa*.

Table S4 DEGs of *PtrXB38-OE* plants in stem.

Table S5 DEGs of *PtrXB38-OE* plants in leaf.

Table S6 DEPs of *PtrXB38-OE* plants in stem.

Table S7 DEGs of *PtrXB38-OE* plants in root.

Table S8 DEPs of *PtrXB38-OE* plants in root.

Table S9 Statistical analysis of genotype × treatment effect by GLMM.

Table S10 PtrXB38-interacting proteins identified in the stem of *Populus tremula* × *Populus alba*.

Table S11 PtrXB38-interacting proteins identified in the root of *Populus tremula* × *Populus alba*.

Please note: Wiley is not responsible for the content or functionality of any Supporting Information supplied by the authors. Any queries (other than missing material) should be directed to the *New Phytologist* Central Office.